

UHP eclogite from western Dabie records evidence of polycyclic burial during continental subduction

BIN XIA^{1,*}, YUNFENG SHANG¹, XIANBIN LU¹, AND YUANBAO WU¹

¹School of Earth Sciences, State Key Laboratory of Geological Processes and Mineral Resources, China University of Geosciences, Wuhan 430074, China

ABSTRACT

Understanding the behavior of continental crust during subduction is important for investigating dynamic processes at convergent plate margins. Although simulations have predicted continental crust may experience multiple burial-partial exhumation cycles during subduction, petrological evidence of these cycles is scarce. In this study at Sidaohe, western Dabie, we combine microstructural observations and mineral chemistry with phase equilibrium modeling, Amp-Pl thermobarometry and Zr-in-rutile thermometry to constrain the P - T evolution for three eclogite samples. All samples have a similar mineral assemblage of garnet + omphacite + symplectite (amphibole + plagioclase \pm clinopyroxene) + quartz, with accessory rutile/ilmenite. Element mapping and analytical traverses across large garnets from two samples show obviously systematic variations in Ca and, less strongly, Mg, Fe, and X_{Mg} [$\text{Mg}/(\text{Mg}+\text{Fe}^{2+})$]. Based on phase equilibrium modeling and calculated isopleths for grossular, pyrope and X_{Mg} in garnet, we show that P first increased from 23.0 to 28.5 kbar, then decreased to 24.0 kbar, before increasing again to a maximum of 30.5 kbar (± 1.0 kbar, 2 sigma error) concomitant with a small increase in T from 580 to 605 °C (± 20 °C, 2 sigma error) at the late prograde stage. These data are interpreted to indicate multiple burial cycles and partial exhumation of eclogite during ongoing continental subduction. After the P_{max} stage, T first increased to a maximum of 664–644 °C at 25.0–20.0 kbar, then decreased to 581–561 °C (± 30 °C, 2 sigma error) at 15.0–10.0 kbar based on results of Zr-in-rutile thermometry. Further decompression and cooling occurred across P - T fields of 590–567 °C at 12.0–10.0 kbar and 520–504 °C (± 40 °C, 2 sigma error) at 8.0 kbar. Fine-grained symplectite (clinopyroxene + plagioclase \pm amphibole) in the matrix is interpreted to have formed after omphacite due to dehydroxylation of nominally anhydrous minerals during decompression from the P_{max} stage. By contrast, formation of coarse-grained symplectite (amphibole + plagioclase) and a veinlet of rutile + quartz that crosscuts one sample may be related to influx of externally sourced H_2O . This study shows that: (1) evidence of cyclic burial and partial exhumation may be retained in low- T eclogite during continental subduction, and (2) fluid contributing to widespread retrogression of eclogite during exhumation may be internally and/or externally sourced.

Keywords: Eclogite, phase equilibrium modeling, multiple burial cycles, continental subduction, western Dabie

INTRODUCTION

Subduction zones play a key role in material recycling between Earth's surface and its interior (Zheng et al. 2012). Based on geological and geophysical observations, and on numerical simulations, a model was developed to understand the dynamics of ocean slab subduction beneath arcs or continents into the mantle (Shreve and Cloos 1986; Cloos and Shreve 1988; Gerya et al. 2002). In this model, a subduction channel develops between the upper and lower plates where a mélange of sediments, crustal fragments and fluid accommodates deformation, metamorphism and metasomatism (Shreve and Cloos 1986). Subsequently, the model was applied to interpret geodynamic processes in continental collision zones (e.g., Zheng et al. 2012; Butler et al. 2013). Similar to the model for oceanic subduction, during

continental subduction detached fragments of continental crust were predicted to undergo multiple burial-exhumation cycles due to convective flow (Gerya et al. 2002; Gerya and Stöckhert 2006; Zheng et al. 2009). However, direct petrological evidence for this behavior is sparse (e.g., Beltrando et al. 2007; Rubatto et al. 2011) and the detailed movements of detached fragments of continental crust during subduction are poorly known.

To understand geodynamic processes operating in continental subduction channels we need a robust determination of the P - T evolution of high-pressure (HP) and ultrahigh-pressure (UHP) rocks (Wei et al. 2010; Li et al. 2016; Xia et al. 2018a; Bovay et al. 2021). Using phase equilibrium modeling and compositional isopleth thermobarometry (Wei et al. 2010; Groppo et al. 2015), we can constrain P - T conditions from rock-forming minerals in eclogite (e.g., garnet, phengite) under the assumption that the chemical composition was not reset, or was only slightly reset, during the post-peak metamorphic evolution (Caddick et

* E-mail: xiabin@cug.edu.cn

al. 2010; Rubatto et al. 2011; Bovay et al. 2021). For instance, studies of garnet with growth zonation from eclogite in the Chinese SW Tianshan (Li et al. 2016) and from schists in the Sevier hinterland, U.S.A. (Harris et al. 2007) revealed episodes of sharp increases and decreases in P , interpreted to represent multiple burial-exhumation cycles. In both cases, the garnet occurs in rocks with relatively low T at the peak stage (<550 °C), which is beneficial for the retention of P - T information in compositionally zoned garnet. However, eclogite in continental subduction zones commonly records higher a T at the peak or during the retrograde stages (>650 °C; Carswell and Zhang 1999), which may result in the removal of early-stage P - T information due to compositional re-equilibration (Liu et al. 2006; Caddick et al. 2010; Groppo et al. 2015; Xia et al. 2018a).

The Sulu-Dabie belt, which formed during the Triassic collision between the Yangzi and Sino-Korean cratons, has been regarded as the typical example for continental subduction (Fig. 1a; Zheng et al. 2012, 2019). However, no petrological evidence supporting a polycyclic burial-exhumation process has been reported from HP-UHP rocks from the Sulu-Dabie belt. In western Dabie, peak temperature for HP-UHP eclogite was constrained to 520–670 °C at 26.0–31.0 kbar (Zhang and Liou 1994; Liu et al. 2004, 2006; Wei et al. 2010), distinctly lower than eclogite from the eastern Dabie (average of 700 ± 50 °C at >28.0 kbar) and Sulu (average of 750 ± 50 °C at 29.0–43.0 kbar) belts (Zhang et al. 2009; Suo et al. 2012; Wu and Zheng 2013; Li et al. 2018; Zheng et al. 2019). In addition, previous studies have shown that garnet from eclogite in western Dabie commonly has growth zonation (Liu et al. 2004, 2006; Wei et al. 2010). Therefore, we infer that early-stage P - T information may have

been retained in garnet from these eclogites. In this study, we determine P - T conditions for the prograde, peak and retrograde stages and construct a complete P - T path for eclogite at Sidaohe, western Dabie. Based on phase equilibrium modeling using compositional isopleth thermobarometry, we report changes in P from eclogite, which we interpret to represent polycyclic burial-partial exhumation processes during continental subduction.

GEOLOGICAL BACKGROUND

In western Dabie (Fig. 1b; also known as the Hong'an block), various types of metabasite (blueschist, greenschist, and eclogite) and serpentinite are mainly enclosed in volumetrically dominant metasedimentary rocks and granitic gneiss as blocks, lenses and occasionally, intercalated layers (Liu et al. 2004). From south to north, based on systematic variations of lithologies and metamorphic grade, six lithotectonic units are subdivided (Fig. 1b; Wei et al. 2010), which are: the Mulanshan greenschist-blueschist unit (peak P - T conditions for garnet-bearing blueschist at 5.0–11.0 kbar, 319–427 °C; Liu et al. 2004), the Hong'an HP eclogite unit (peak P - T conditions for eclogite at 19.0–26.0 kbar, 485–585 °C; Liu et al. 2004; Lou et al. 2013), the Xinxian UHP eclogite unit (P_{\max} stage P - T conditions for eclogite at 28.0–32.0 kbar, 520–670 °C; Zhang and Liou 1994; Liu et al. 2004, 2006; Wei et al. 2010), the Huwan HP eclogite unit (peak P - T conditions for eclogite at 18.0–23.0 kbar, 540–630 °C; Liu et al. 2004; Ratschbacher et al. 2006), the Balifan mélange unit (P - T conditions for a mylonitized quartz-feldspathic schist at 9.0–10.0 kbar, 458–516 °C; Liu et al. 2004) and the Nanwan flysch unit. The variation of metamorphic grade and the architecture of units has been interpreted to represent a huge anticline with UHP rocks at the core and HP rocks at the two limbs, similar to the eastern Dabie belt (Hacker et al. 2000; Liu et al. 2004).

In western Dabie, geochronological studies on eclogite and country rocks have constrained the prograde stage metamorphism to occur at 239–226 Ma, the peak UHP eclogite facies metamorphism at ~226 Ma, the early retrograde eclogite facies metamorphism at 216–213 Ma and the later retrograde amphibolite facies metamorphism at ~212 Ma (Wu and Zheng 2013 and references therein). These ages are comparable to the eastern Dabie and Sulu belts, indicating they are a huge continuous Triassic orogenic belt. However, in the western segment of the Huwan HP eclogite unit, late Carboniferous ages of ~310 Ma have been reported for eclogite and its country rock gneisses (Wu et al. 2009; Liu et al. 2011). Based on geochemical signatures of some eclogite showing oceanic crust affinity, these ages were interpreted to represent an early oceanic subduction prior to the Triassic continental collision (Wu and Zheng 2013).

ANALYTICAL METHODS AND SAMPLING

Analytical methods

Initial mineral analyses and element mapping for symplectite were performed using a JEOL-8230 electron probe microanalyzer with 4 wavelength-dispersive spectrometers (WDS) at the Center for Global Tectonics, School of Earth Sciences, China University of Geosciences (Wuhan). The operating conditions were 15 kV acceleration voltage, 20 nA beam current, and 1 μ m beam diameter for garnet and clinopyroxene and 5–10 μ m beam diameter for amphibole and plagioclase. Raw X-ray intensities were corrected using a ZAF (atomic number, absorption, fluorescence) correction procedure. A series of natural and synthetic standard peak intensity (SPI) standards were used and changed based on the analyzing minerals. The following

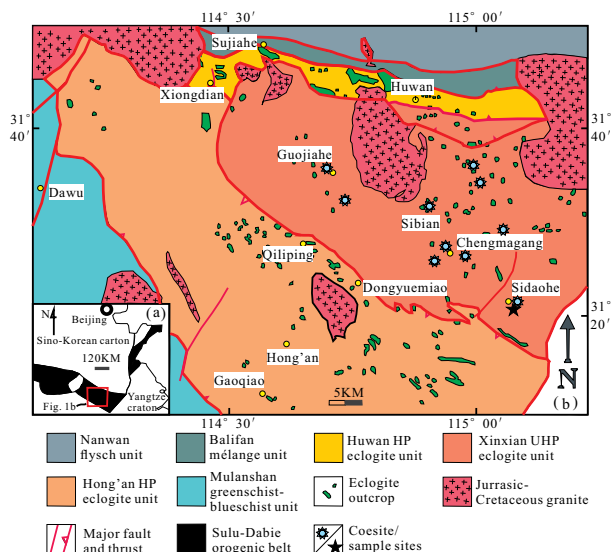


FIGURE 1. (a) Tectonic framework of the Sulu-Dabie orogen in central China. It is located between the Yangtze craton to the south and the Sino-Korean craton to the north. (b) Geological map of the western Dabie (modified from Wei et al. 2010). Based on lithologies and metamorphic grade, western Dabie is subdivided into 6 units. From south to north, they are: the Mulanshan greenschist-blueschist unit, the Hong'an HP eclogite unit, the Xinxian UHP eclogite unit, the Huwan HP eclogite unit, the Balifan mélange unit and the Nanwan flysch unit. (Color online.)

standards were used: sanidine (K), pyrope garnet (Fe, Al), diopside (Ca, Mg), jadeite (Na), rhodonite (Mn), olivine (Si), rutile (Ti). Elements in unknown samples were all determined within about 2% relative based on analyses of secondary standards. Representative results are given in Online Materials¹ Tables OM1 and OM2.

Backscattered electron (BSE) images and energy-dispersive spectrometer (EDS) analyses were obtained using an FEI Quanta 200 scanning electron microscope (SEM) equipped with an EDAX EDS system at the State Key Laboratory of Geological Process and Mineral Resources, China University of Geosciences (Wuhan). The images were obtained at an accelerating voltage of 20 kV with a spot size of 200–400 nm, an emission current of ~100 μ A, and a working distance of 11–12 mm.

Trace element analyses of rutile grains were performed by the laser ablation-inductively coupled plasma-mass spectrometry (LA-ICP-MS) method at Wuhan Sample Solution Analytical Technology Co. Ltd. Laser sampling was performed using a GeolasHD laser ablation system (wavelength of 193 nm). We used 80 mJ laser energy, 32 μ m spot size, and a 5 Hz frequency for the analyses. An Agilent 7900 ICP-MS instrument was used to acquire ion-signal intensities. NIST610, BHVO-2G, BIR-1G, and BCR-2G were used as external standards for trace element analysis. Off-line selection and integration of background and analyzed signals, time-drift correction and quantitative calibration for trace element analysis and U-Pb dating were performed by ICP-MSDataCal (Liu et al. 2008). For the detailed procedure, please reference Liu et al. (2008). For inclusions and matrix rutile the microbeam analyses were focused on their central part, for megacrystal rutile two profile analyses were performed. The results are shown in Online Materials¹ Table OM3.

The whole rock compositions were analyzed at the State Key Laboratory of Geological Processes and Mineral Resources, China University of Geosciences (Wuhan) using X-ray fluorescence (XRF) of fused glass disks. The samples were first crushed to <60 mesh in a corundum jaw crusher, then to <200 mesh in an agate mill. Then, 0.5 g of rock powder, together with 5 g of flux (Li₂B₄O₇:LiBO₂ = 12:22) were fused in a high-frequency melting furnace for 11 min at ~1050 °C in 95% Pt–5% Au crucibles. The melt was swirled repeatedly to ensure complete dissolution and homogenization of the material, and then poured into a mold to form a thin, flat-surfaced disk (34 mm diameter). The loss-on-ignition (LOI) was measured on dried rock powder by heating in a pre-heated corundum crucible to 1000 °C for 90 min and recording the weight loss. XRF analysis was carried out on a Shimadzu XRF-1800 sequential X-ray fluorescence spectrometer, using a Rh-anode X-ray tube with a voltage of 40 kV and current of 70 mA. Calibration curves used for quantification were produced by bivariate regression of data from ~63 reference materials encompassing a wide range of silicate compositions. The measurement procedure and data quality were monitored by repeated samples (one in eight samples), USGS standard AGV-2 and Chinese National standards GSR-1 and GRS-7.

Sampling

In this study, eclogite samples were collected at Sidaohe (115°37'33.33"E, 31°20'32.67"N) in the Xinxian UHP eclogite unit (Fig. 1b). Eclogite occurs as block (4–6 m in diameter) and is enclosed in garnet-bearing felsic gneiss (Fig. 2a). From center to rim, it was more severely retrograded with more abundant quartz veins developed at the edge (Figs. 2a and 2b).

To qualify *P-T* evolution of the eclogite at Sidaohe, we chose three samples (Sdh-1, Sdh-2, and DB17-06) for detailed petrological analysis. Sdh-1 and Sdh-2 were selected for phase equilibrium modeling, while Sdh-1 and DB17-06 were chosen for rutile trace element analysis.

PETROLOGY

All samples at Sidaohe, western Dabie show various retrogression in thin sections (Figs. 2c, 2d, and 3). Both eclogite Sdh-1 and Sdh-2 show a granoblastic texture in the scanned thin section (Fig. 2c) and have a similar mineral assemblage of garnet (43–48 vol%) + omphacite (1–3%) + symplectite of Pl \pm Amp \pm Cpx (37–42%) + quartz (10–15%) and accessory rutile/ilmenite (2–3%) (Fig. 2c) [note that mineral abbreviations in this study follow Whitney and Evans (2010)]. The eclogite Sdh-1 has slightly more quartz but less symplectite than Sdh-2. Sample DB17-06, with the quartz veinlet, has been more severely retrogressed with less garnet relics but more Pl \pm Amp \pm Cpx symplectite in the matrix (Fig. 2d). The veinlet mainly consists of oriented coarse

quartz and rutile and Pl \pm Amp \pm Cpx symplectite (Fig. 2d).

Porphyroblastic garnet (anhedral to subhedral, 0.5–3.0 mm in diameter) is cut by fractures filled with dominantly fine-grained amphibole and/or fibrous Amp + Pl \pm Rt/Ilm symplectite (Figs. 3a, 3b, 3f, and 3h). Coronas of Amp \pm Pl develop along garnet rims (Figs. 3h and 3i). Inclusions in garnet are mainly omphacite, quartz, Pl \pm Amp \pm Cpx symplectite, with rare epidote, amphibole, rutile/ilmenite, and apatite (Figs. 3a–3e and 3k). Traverses from core to rim (Figs. 4a and 4b) and element mapping (Fig. 4c–4f) across a large porphyroblastic garnet from both Sdh-1 and Sdh-2 show obvious zoning of Ca and, less strongly, Mg, Fe, and X_{Mg} , but no Mn zoning. For Sdh-1, Grs first decreases from 31 to 25–26 mol% from core to mantle, then increases to 28–29 mol% before decreasing again to 20–21 mol% from mantle to rim. Alm varies antithetically with Grs but consistently with Pyr (Fig. 4a). From core to rim, Alm first slightly increases from 50 to 52 mol%, then decreases to 50 mol% before increasing again to 55 mol%; Prp first increases from 18 to 21–22 mol%, then decreases to 18–20 mol% before increasing again to 23 mol%; X_{Mg} varies from 0.26 to 0.30. For Sdh-2, from core to rim, Grs first decreases from 29 to 24–25 mol%, then increases to 28–29 mol% before decreasing again to 23–24 mol%; Alm first increases from 50 to 52–53 mol%, then decreases to 50 mol% before increasing again to 54 mol%; Prp first increases from 18 to 21–22 mol%, then decreases to 20 mol% before increasing again to 22 mol%. X_{Mg} varies from 0.25 to 0.29–0.30. Sps varies little from core to rim (1–2 mol%) for both samples (Figs. 4a and 4b).

Omphacite is only preserved as inclusions in garnet (Figs. 3c and 3e). In the matrix, it was completely replaced by Pl \pm Amp \pm Cpx symplectite showing short prismatic or granular shapes (Figs. 2c, 3g, and 3h). The reaction was inferred to be $Omp \pm H_2O \rightarrow Pl \pm Amp \pm Cpx$, as has been evidenced by the symplectite partially replacing omphacite in garnet (Fig. 3c). Intergrowths of Cpx, Pl, and/or Amp are generally perpendicular to the reaction front (Figs. 3c, 3g, and 5a–5g). Previous studies have shown that symplectite usually grew from the original omphacite margins to the reaction front and the thickness of the lamellae usually decreases with decreasing temperature (Joanny et al. 1991; Waters 2003; Lanari et al. 2013). Therefore, in the matrix, we define Cpx-bearing symplectites of Cpx1 + Amp1 + Pl1 (mineral grain sizes 50–100 μ m in diameter; Figures 3d, 3e, 3g, 3h, 3j, 5a, 5b, and 5d–5k) as Sym1 and Cpx2 + Pl2 (commonly <20 μ m in diameter; Figs. 3g, 3h, 5a, and 5b) as Sym2. For the Cpx-absent symplectite of Amp3 + Pl3 (commonly >100 μ m; Figs. 3h and 3i) formed at later amphibolite facies metamorphism (Martin 2019), we define it as Sym3. For both Sdh-1 and Sdh-2, omphacite included in garnet has constant X_{Id} of 42–45 mol% while Cpx1 in Sym1 has lower X_{Id} of 12–26 mol% (Fig. 6a). Composition of Cpx2 in Sym2 was not measured due to its small dimensions (<10 μ m in diameter).

Amphibole in eclogite is found in three textural positions. (1) As inclusions in garnet (Figs. 3a and 3i). For Sdh-1 and Sdh-2, Amp has comparable $^c(Al + Fe^{3+} + 2Ti)$ of 1.29–1.93 apfu and $^a(Na + K + 2Ca)$ of 0.35–0.70 apfu (23 O basis), mostly ranging from sadanagaite to tschermakite, with only one pargasite (Fig. 6b; Hawthorne et al. 2012). (2) Together with Pl constituting Sym1 (Amp1; Figs. 5a and 5b) and Sym3 (Amp3; Figs. 3g, 3h,

and 3i). For Sdh-1, Amp1 has $^c(\text{Al} + \text{Fe}^{3+} + 2\text{Ti})$ of 0.89–1.41 apfu and $^a(\text{Na} + \text{K} + 2\text{Ca})$ of 0.46–0.58 apfu, ranging from pargasite to magnesiohornblende; Amp3 has $^c(\text{Al} + \text{Fe}^{3+} + 2\text{Ti})$ of 0.79–0.94 apfu and $^a(\text{Na} + \text{K} + 2\text{Ca})$ of 0.15–0.27 apfu, is magnesiohornblende. For Sdh-2, Amp1 has $^c(\text{Al} + \text{Fe}^{3+} + 2\text{Ti})$ of 1.48 apfu and $^a(\text{Na} + \text{K} + 2\text{Ca})$ of 0.50 apfu, is magnesiohornblende; Amp3 has $^c(\text{Al} + \text{Fe}^{3+} + 2\text{Ti})$ of 0.59–1.03 apfu and $^a(\text{Na} + \text{K} + 2\text{Ca})$ of 0.07–0.21 apfu, is magnesiohornblende (Fig. 6b). And (3) rimming garnet (Figs. 3i and 3j) or together with Pl and Rt/Ilm in cracks in garnet (Fig. 3f), has $^c(\text{Al} + \text{Fe}^{3+} + 2\text{Ti})$ of 1.61–1.77 apfu and $^a(\text{Na} + \text{K} + 2\text{Ca})$ of 0.66–0.71 apfu, belonging to Sadanagaite (Fig. 6b).

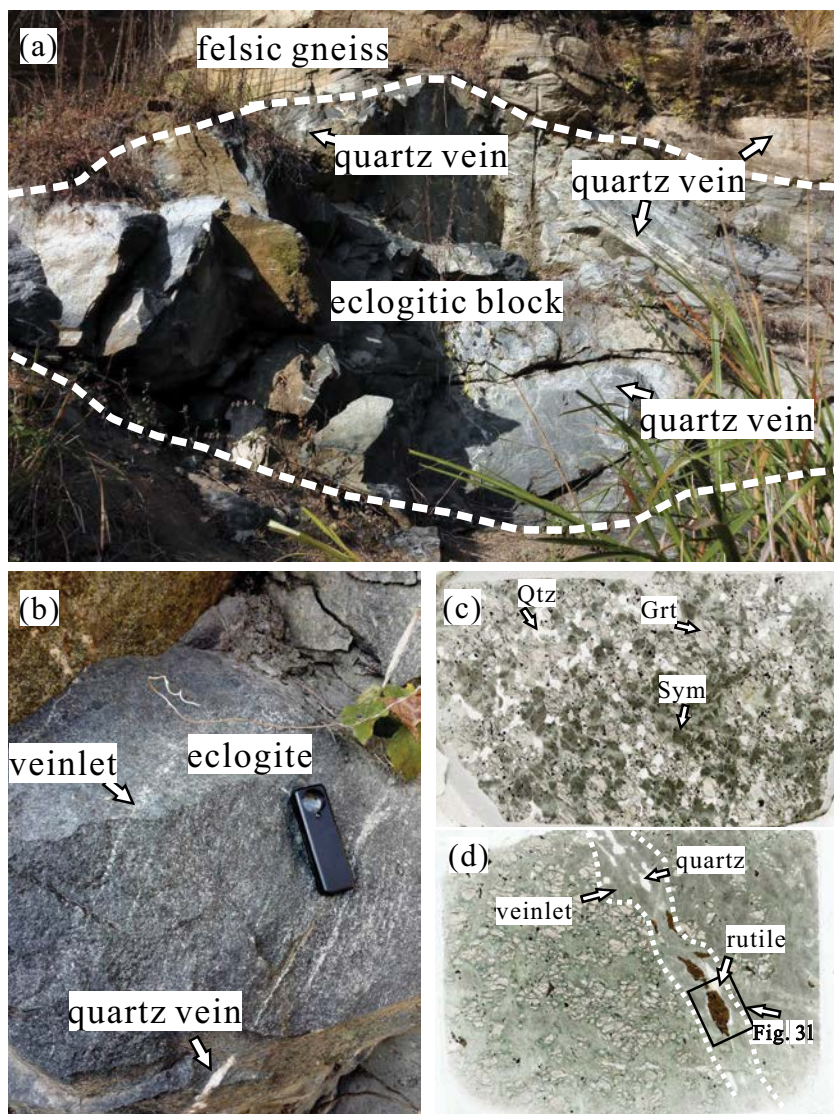
Plagioclase in both Sym1 and Sym3 is albite with $\text{Ab}_{0.92-0.99}$ (mean 0.96). Epidote is included in garnet but absent in the matrix (Fig. 3a). It has Fe^{3+} of 0.61.

Rutile shows various occurrences in thin sections: as inclusions in garnet (30–100 μm ; inclusion Rt as type 1; Fig. 3i); in the matrix (100–300 μm ; matrix Rt as type 2; Figs. 3j and 3k) and as megacrystals in the veinlet (500–4000 μm ; megacrystal rutile as

type 3; Figs. 2d and 3l). Most of rutile grains have been partially replaced by ilmenite along rims or fractures (Figs. 3j, 3k, and 3l).

Based on the above petrographic observations and mineral compositions, several stages in the metamorphic evolution of the eclogite at Sidaohe, western Dabie may be inferred. Evidence of the prograde metamorphic stage (M0) is recorded by garnet and its inclusions of omphacite, amphibole, quartz, epidote and rutile (type 1). $\text{Pl} \pm \text{Amp} \pm \text{Cpx}$ symplectite in the matrix is interpreted to represent former omphacite and is a typical decompression-related texture in eclogite (Joanny et al. 1991). The peak stage (M1) mineral assemblage is inferred to be $\text{Grt} + \text{Omp} + \text{Qtz} + \text{Rt}$ (type 2). The retrograde metamorphic stage (M2) is represented by the breakdown of Omp to form Sym1 ($\text{Cpx1} + \text{Amp1} + \text{Pl1}$) and Sym2 ($\text{Cpx2} + \text{Pl2}$). The late retrograde metamorphic stage (M3) is represented by Sym3 ($\text{Amp3} + \text{Pl3}$) replacing Sym1 and Sym2 (Fig. 3e), amphibole/plagioclase and chlorite replacing garnet (Figs. 3c and 3g). Megacrystal rutile (type 3) in veinlets may be formed prior to stage M3, whereas ilmenite replacing rutile in the matrix may form at this stage.

FIGURE 2. (a) Eclogitic block enclosed in the host garnet-bearing felsic gneiss. Eclogite is strongly retrogressed from the center toward the rim. Abundant quartz veins are at the edge of the block, with less in its interior. (b) Small veinlets in the center of the block where eclogite Sdh-1 was sampled. Close to veinlet, eclogite was more strongly retrogressed. (c) Thin section for Sdh-1 showing bimineralic texture with omphacite in the matrix completely replaced by $\text{Pl} \pm \text{Amp} \pm \text{Cpx}$ symplectite. (d) Thin section for DB17-06 with veinlet of megacrystal rutile and quartz cross-cutting eclogite. (Color online.)



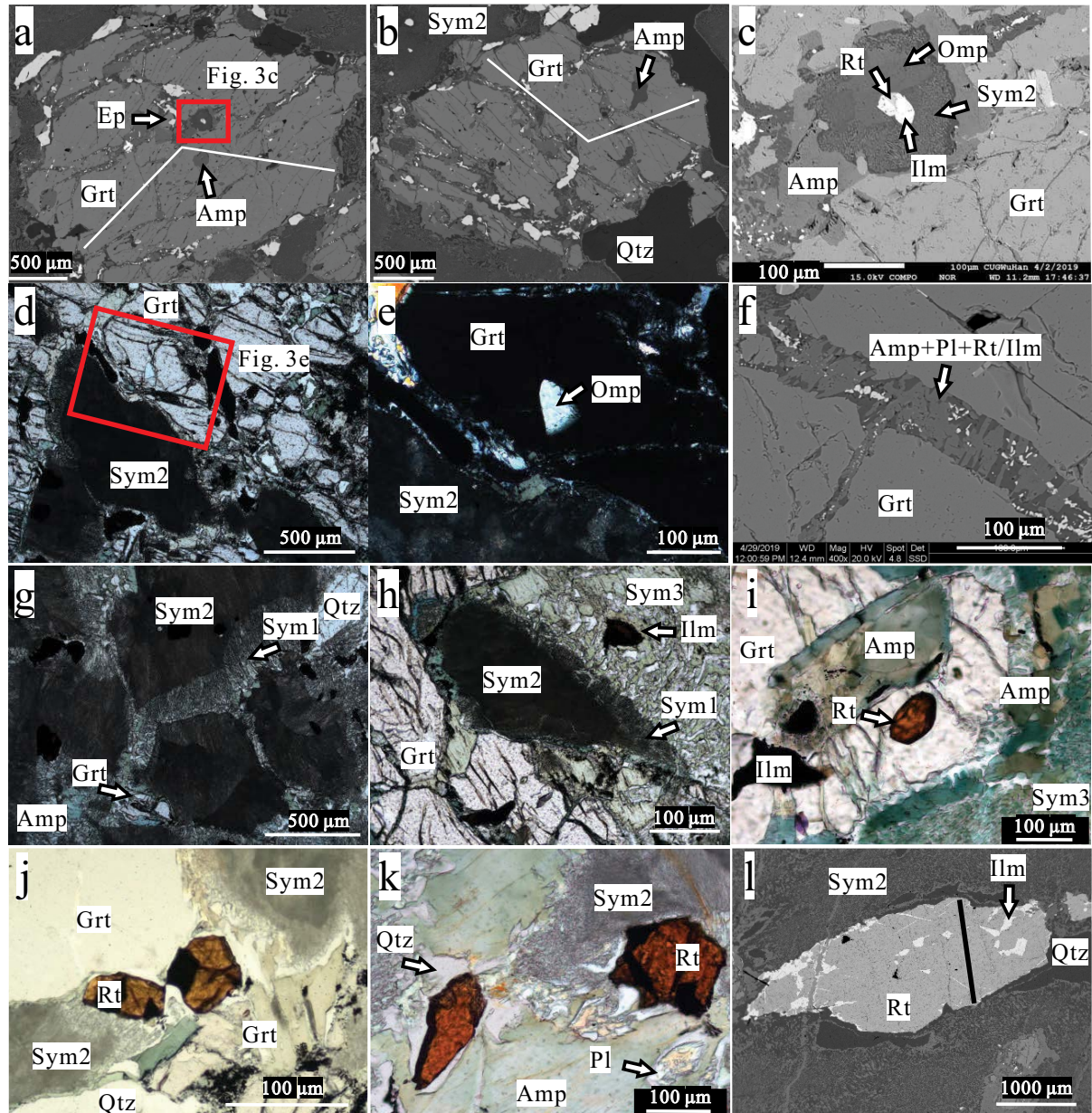


FIGURE 3. Photomicrographs showing the mineralogy and microstructures of eclogite in BSE images (**a, b, c, f, l**), under cross-polarized light (**e**) and plane-polarized light (**d, g, h, i, j, k**). (**a**) Subhedral garnet porphyroblast from Sdh-1 with inclusions of Ep, Amp, Omp, and Qtz; cracks in garnet are mainly filled with Amp + Pl + Rt/IIm. Traverses of point analyses roughly follow the solid white line. (**b**) Subhedral garnet porphyroblast from Sdh-2. Traverses of point analyses roughly follow the solid white line. (**c**) Omphacite inclusion in garnet of **a**. Omphacite was partly replaced by Cpx + Pl symplectite (Sym2) which was rimmed by coarse Amp. (**d** and **e**) Omphacite inclusion in garnet. In the matrix, Pl ± Amp ± Cpx symplectite shows short prismatic or granular shapes interpreted to be pseudomorphs after omphacite. (**f**) Fractures in garnet filled with fibrous Amp + Pl ± Rt/IIm symplectite. (**g** and **h**) Cpx + Pl + Amp (Sym1), Cpx + Pl (Sym2) and Amp + Pl (Sym3) symplectites in the matrix showing short prismatic shape; (**i**) Rutile inclusions in garnet (type 1). (**j**) Rutile as single grains in the matrix abutting garnet (type 2). (**k**) Rutile in the matrix surrounded by Qtz + Amp or Pl ± Amp ± Cpx symplectite (type 2). (**l**) Megacrystal rutile in quartz veinlet crosscutting eclogite (type 3). Rutile has been partially replaced by ilmenite along rims or fractures. (Color online.)

PHASE EQUILIBRIUM MODELING

To constrain peak P - T conditions and metamorphic processes for the eclogite at Sidaohe, western Dabie, phase equilibrium modeling was performed using THERMOCALC software (version 3.40, updated in March 2014) and the associated internally consistent thermodynamic data set ds62 (Holland and Powell 2011; updated in November 2016). The chemical system used for modeling is (Mn)NCFMASHTO [(MnO)-Na₂O-CaO-FeO-MgO-Al₂O₃-SiO₂-H₂O-TiO₂-O] system. A - x relationships used in the modeling are as follows: garnet (White et al. 2014); clinopyroxene and amphibole (Green et al. 2016); plagioclase (Holland and Powell 2003); and epidote (Holland and Powell 2011). Rutile,

sphene, lawsonite, kyanite, quartz, and H₂O are considered to be pure phases.

In the modeling to constrain the prograde to peak P - T evolution for the eclogites Sdh-1 and Sdh-2, the whole-rock compositions obtained by XRF were used after correction of the CaO content for the P₂O₅ contained in apatite (Table 1). The O content (equals to Fe₂O₃ in molar percent) was calculated from the whole-rock composition of eclogite sampled in the same locality of this study by Yan et al. (2005). In their study using wet chemistry, eclogite and retrograded eclogite gave a consistent Fe₂O₃ (in molar percent)/FeO⁺ (in mol%) ratio of 7.5%. H₂O was set to be in excess based on the assumption that the prograde evolution may be H₂O saturated

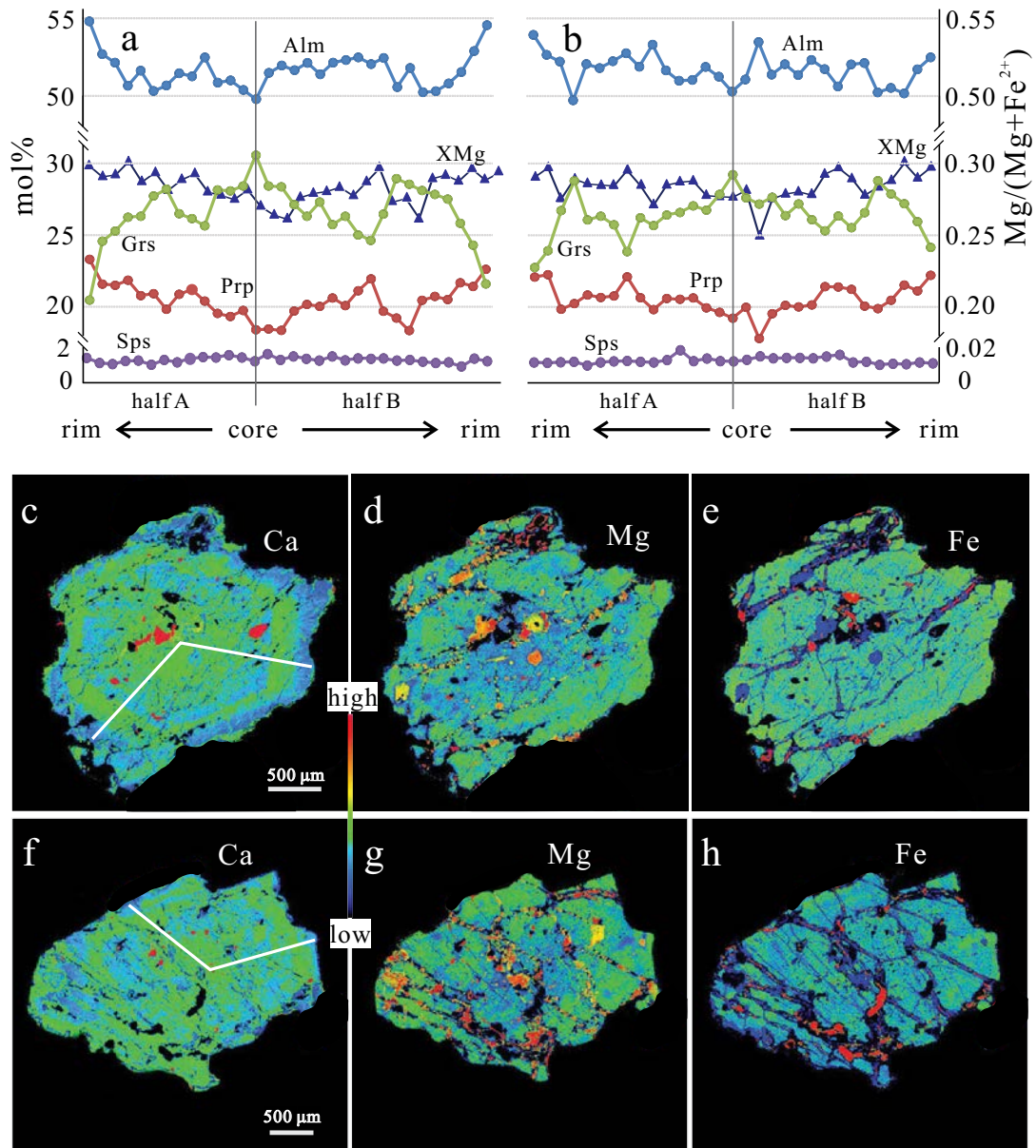


FIGURE 4. Traverses of point analyses for garnet from (a) Sdh-1 and (b) Sdh-2. Half A and B represent analyses for one half and the other half of the garnet, respectively. (c-d) Element mapping of Ca and Mg for a large porphyroblastic garnet from Sdh-1; the dotted lines may represent garnet zoning patterns. (e-f) Ca and Mg element mapping for a large porphyroblastic garnet from Sdh-2; the dotted lines represent suggested garnet zoning patterns. (Color online.)

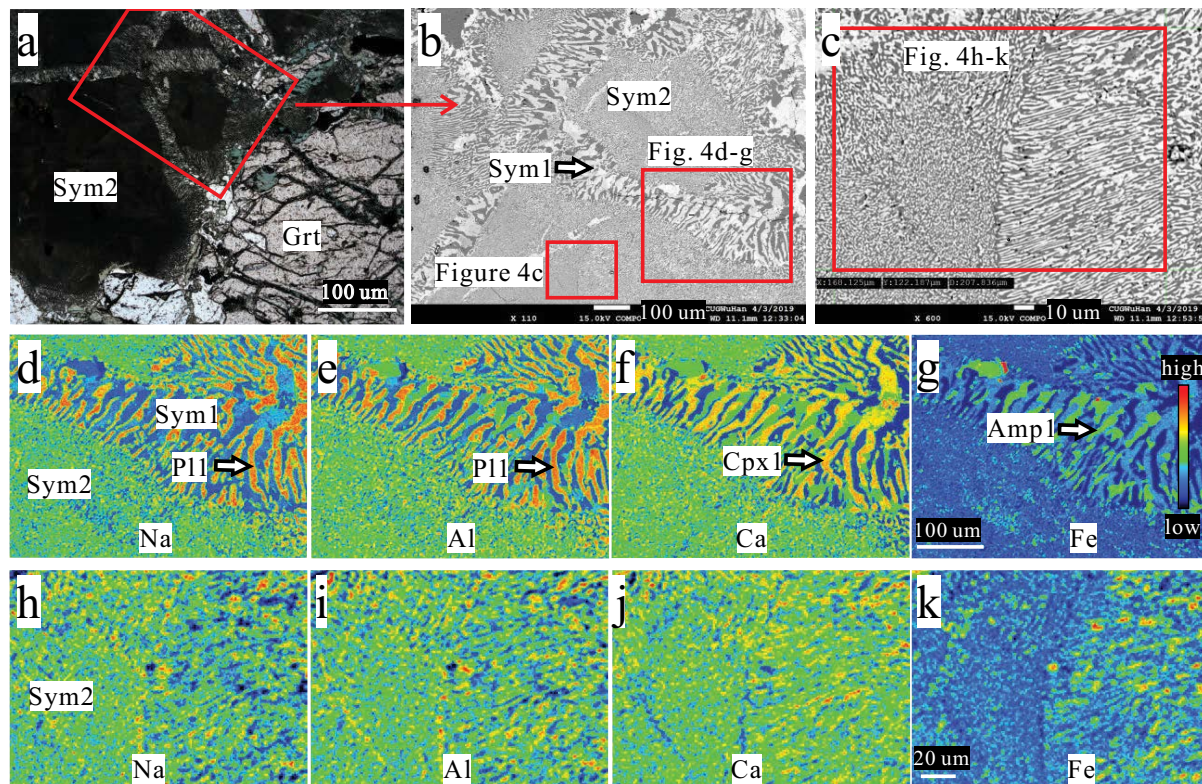
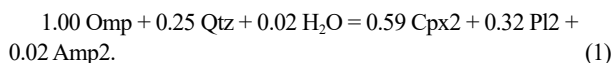


FIGURE 5. Photomicrographs showing the microstructures of symplectite in Sdh-1 under plane-polarized light (a) and in BSE images (b and c). Element maps of Sym1 (d–f) and Sym2 (h–k) showing intergrowths of Cpx, Pl, and/or Amp generally oriented perpendicular to the reaction front. From Sym1 to Sym2, Amp (in volume content) decreases while Cpx increases (d–k). (Color online.)

considering the progressive transition from a mineral assemblage dominated by hydrous minerals (e.g., epidote, lawsonite, chlorite, and glaucophane) to one dominated by anhydrous minerals (e.g., garnet and omphacite), and the observed abundance of hydrous minerals as inclusions in garnet. To constrain P - T conditions for the retrograde stage forming Cpx + Pl + Amp symplectites after omphacite, the effective bulk-rock composition calculated from the equilibrated reaction combined with mineral compositions was used in the phase equilibrium modeling. The balanced reaction forming Sym1 after omphacite using the least square method (software PCalc2.3 by Godard 2009) applied to compositions of Omp, Cpx1, Pl1, and Amp1 is as follows:



TiO₂ in the effective bulk composition is same as the value for modeling in Figure 7a and H₂O was set to be in excess (Table 1). Sample compositions (in wt%) and corrected or modified bulk compositions (in mol%) used for phase equilibrium modeling are given in Table 1.

Prograde to peak metamorphic stages

P - T pseudosections constraining the prograde to peak P - T evolution for the eclogites Sdh-1 (Fig. 7a) and Sdh-2 (Fig. 7b) were calculated in the MnNCFMASHTO system using the bulk

compositions in Table 1 for the P - T range 12.0–32.0 kbar and 500–700 °C. Both calculations show similar topology for phase relations. For instance, lawsonite is present in the top-left phase assemblage fields and is replaced by epidote at $P < 21.0$ kbar at $T < 610$ –615 °C, and by Grt + Omp ± Ky at $T > 610$ °C; glaucophane/hornblende is replaced by Grt + Omp ± Ky at $P > 20.5$ kbar and $T > 590$ –595 °C. However, kyanite is modeled to be present at P of 19.5–26.0 kbar at $T > 610$ °C in Figure 7a, but is absent in Figure 7b; epidote is modeled to be present across the whole T range in Figure 7a, but is absent at $T > 640$ °C in Figure 7b.

Isoleths for Grs (18–38 mol%), Prp (7–26 mol%), and X_{Mg} (0.25–0.30) in garnet and $j(\text{o})$ [$\text{Na}/(\text{Na}^+\text{Ca})$, 0.45–0.54] in omphacite have been calculated for most of the modeled P - T range (Figs. 7c and 7d). The results show that Grs values in garnet roughly decrease while Prp and X_{Mg} values roughly increase with increasing pressure and temperature (Figs. 7c and 7d). In the phase assemblage fields of Grt + Omp + Lws + Gln + Coe/Qtz + Rt + H₂O, the measured Grs, Prp and X_{Mg} in garnet from Sdh-1 (Grs = 0.31–0.21, Prp = 0.18–0.23, and X_{Mg} = 0.26–0.30) and Sdh-2 (Grs = 0.29–0.23, Prp = 0.18–0.22, and X_{Mg} = 0.25–0.30) define comparable P - T fields of 23.0–30.5 kbar, 585–605 °C, and 24.5–29.5 kbar, 580–600 °C, respectively (Figs. 7c and 7d). From garnet core to rim, P first increases from 23.0 to 28.5 kbar, then decreases to 24.0 kbar before increasing again to 30.5 kbar concomitant with a small increase in T from 580 to 605 °C (Figs. 7e and 7g). In the phase assemblage fields of Grt + Omp + Lws ±

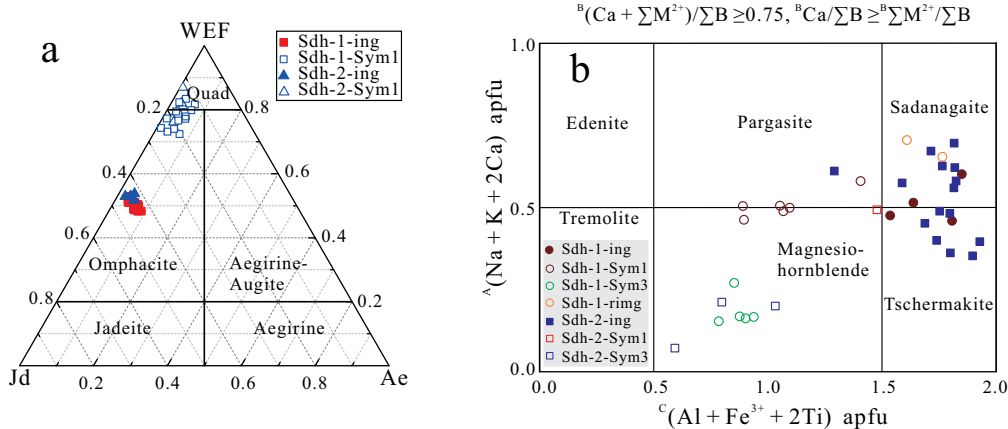


FIGURE 6. Compositions of omphacite and amphibole from the eclogite Sdh-1 and Sdh-2. **(a)** Compositions of omphacite. WEF represents end-members for Wo (wollastonite), En (enstatite), and Fs (ferrosilite) after Morimoto et al. (1988). **(b)** Classification of amphibole with various occurrences (after Hawthorne et al. 2012). Ing = as inclusions in garnet; ring = rimming garnet. (Color online.)

TABLE 1. Whole-rock compositions (in wt%) together with modified bulk compositions (in mol%) used for phase diagram calculations for eclogite at Sidaohe, western Dabie

Samples	Figures	H ₂ O	SiO ₂	Al ₂ O ₃	CaO	MgO	FeO (Fe ^O)	K ₂ O	Na ₂ O	TiO ₂	MnO	Fe ₂ O ₃ (O)	P ₂ O ₅
Primary bulk-rock composition (wt%)													
Sdh-1	*		50.99	13.97	9.54	5.52	14.28	0.03	2.87	2.46	0.22	*	0.39
Sdh-2	*		48.02	13.73	9.99	6.04	14.85	0.04	2.87	2.32	0.21	*	0.43
Corrected bulk-rock composition (mol%)													
Sdh-1	7a and 7c	excess	54.53	8.80	10.34	8.80	11.49	0.02	2.97	1.98	0.19	0.86	
	8a	excess	57.59	6.18	11.82	10.98	4.80	0.00	5.65	1.99	0.00	0.98	
	8b	0.00	57.59	6.18	11.82	10.98	4.80	0.00	5.65	1.99	0.00	0.98	
		2.00	56.43	6.06	11.59	10.76	4.71	0.00	5.54	1.95	0.00	0.96	
Sdh-2	7b and 7d	excess	52.22	8.80	10.98	9.79	12.15	0.03	3.02	1.90	0.19	0.91	

Note: For the modified bulk compositions, Fe^O represents total iron. Oxygen (in mol%) is equal to Fe₂O₃ (in mol%). * null values.

Gln + Coe/Qtz + Rt + H₂O, isopleths for j(o) of omphacite have steep positive slopes with j(o) values increasing with temperature. In these fields, the measured j(o) of omphacite correspond to *T* ranges of 600–650 °C for Sdh-1 [j(o) = 0.52–0.55] and 595–630 °C for Sdh-2 [j(o) = 0.49–0.51] at 25.0–30.0 kbar, respectively. The inferred peak stage (M1) mineral assemblage characterized by Grt + Omp (represented by Pl ± Amp ± Cpx symplectite) + Coe/Qtz + Rt corresponds to the modeled phase assemblage fields of Grt + Omp + Coe/Qtz + Rt + H₂O, defining temperatures of >640 °C in Figure 7a and >615 °C in Figure 7b at *P* > 19.5 kbar, respectively. In combination with the *P*–*T* conditions constrained by isopleths of Grs and Prp in garnet and j(o) of omphacite, a heating process after the *P*_{max} stage may be inferred (Fig. 7f).

Retrograde metamorphic stage

A *P*–*T* pseudosection constraining the retrograde *P*–*T* evolution was calculated for the eclogite Sdh-1 in the NCFMASHTO system using the effective bulk composition in Table 1 for the *P*–*T* range 5.0–25.0 kbar and 450–650 °C (Fig. 8a). In Figure 8a, the observed mineral assemblage in Sym1 corresponds to the modeled phase assemblage fields of O/Dio + Hbl + Pl ± Qtz + Rt + H₂O, defining *P* of 5.0–13.0 kbar at the modeled *T* range. In these fields, j(o) values in omphacite increase with increasing pressure and the maximum j(o) content in the symplectitic Cpx2 from Sdh-1 (0.28) and Sdh-2 (0.30) corresponds to pressures of 10.5–11.5 kbar and 11.0–12.0 kbar at 580–650 °C, respectively. The lower j(o) content (0.10–0.27) in omphacite may indicate

► **FIGURE 7.** **(a and c)** *P*–*T* pseudosection for the eclogite Sdh-1. ① Grt Dio Gln Lws Spn, ② Grt Gln Lws Ep Spn, ③ Grt Gln Lws Dio Omp Ep, ④ Grt Gln Lws Dio Omp Ta, ⑤ Grt Lws Omp Ky, ⑥ Grt Gln Omp Ky, ⑦ Grt Gln Omp Ky Ep, ⑧ Grt Gln Omp Ep Spn, ⑨ Grt Gln Lws Dio. **(b and d)** *P*–*T* pseudosection for the eclogite Sdh-2. ① Grt Dio Gln Lws Spn, ② Grt Gln Lws Ep Spn, ③ Grt Gln Lws Dio Ep, ④ Grt Dio Gln Ep Spn, ⑤ Grt Gln Dio Omp Lws Ep, ⑥ Grt Gln Dio Ep, ⑦ Grt Gln Dio Omp Lws Ta, ⑧ Grt Gln Dio Lws, ⑨ Grt Omp Lws. **(e)** Variations of *P* defined by isopleths of Grs in Grt from core to rim. **(f)** Compilation of the inferred *P*–*T* evolution from the later prograde to the *P*_{max}, then to the *T*_{max} stages for both *P*–*T* pseudosections for Sdh-1 and Sdh-2. The whole rock compositions are given in Table 1. “cg” represents calculated isopleths for Grs in garnet, “mg” represents calculated isopleths for Prp in garnet, xmg represents calculated isopleths for X_{Mg} in garnet, and “jo” represents calculated isopleths for j(o) of omphacite. Lws-Ec represents lawsonite eclogite facies, Ep-Ec represents epidote eclogite facies, Amph-Ec represents amphibolite facies, Ep-Bs represents epidote blueschist facies, EA represents epidote amphibolite facies, AM represents amphibolite facies, HGR represents high-pressure granulite facies (after Liou et al. 2004). In this study, according to *a*–*x* models of amphibole for modeling phase diagram using Thermocalc, glaucophane is defined to have high *z* (0.8–1, Na on the M4 site) and *y* (0.9–1, octahedral Al) combined with low *a* (0–0.2, A-site Na) and *c* (0–0.2, Ca), whereas hornblende is defined to have high *a* (0.2–0.6), *y* (0.2–0.6), and *c* (0.6–0.9). (Color online.) (See next page.)

a decrease of P during further exhumation retrogression.

To evaluate H_2O influence on the formation of Sym1, we calculated a P - M_{H_2O} pseudosection for the eclogite Sdh-1 in the NCFMASHTO system using the bulk composition in Table 1 at $T = 580^\circ C$ for the P range of 5.0–25.0 kbar (Fig. 8b). The H_2O content ranges from 0.00 to 2.00 mol%. In Figure 8b, free H_2O is present in fields with M_{H_2O} above 1.12 mol% and P below 21.5 kbar (the red solid line as the H_2O -saturation boundary). The phase assemblage fields of Dio + Hbl + Pl \pm Omp \pm Qtz \pm H_2O develop at P below 11.0 kbar and M_{H_2O} above 0.56 mol%. Along decompression process during retrogression, eclogite may evolve along the yellow dotted line from A to D with M_{H_2O} content of ~ 1.12 mol% at $P < 11.0$ kbar. We infer H_2O in the bulk rock saturating Sym1 may be ~ 1.12 mol%, corresponding to 0.4 wt%.

AMP-PL THERMOBAROMETRY

In this study, we use Amp-Pl thermobarometry to constrain P - T conditions for the formation of Sym1 with Cpx and Sym3 without Cpx during retrogression. In this study, we calculate temperature for the formation of Sym1 at 12.0 kbar based on the modeling results in Figure 8a. On the other hand, considering the lower Al_2O_3 content in Amp3 than Amp1 in Sym1 which may yield a P difference of ~ 4.0 kbar using the barometry of Schmidt (1992), we calculate T for the formation of Sym3 at 8.0 kbar, similar to that of Martin (2019). The calculation uses the Amp-Pl thermometry B (edenite + albite = richterite + anorthite) by Holland and Blundy (1994). The results show that T for Sym1 (calculated at fixed Ab of 0.96) ranges from 567–590 $^\circ C$ and for Sym3 (calculated at fixed Ab of 0.97) ranges from 504–520 $^\circ C$, respectively. Uncertainties for these results could be $\pm 40^\circ C$ within 2 sigma error (Holland and Blundy 1994).

TRACE ELEMENT COMPOSITION OF RUTILE AND ZR-IN-RUTILE THERMOMETRY

Trace element analyses were applied to rutile from the samples Sdh-1 and DB17-06. Figure 9 shows Nb/Ta vs. Nb, Ta, and Zr, and Zr vs. Sc, U and Hf characteristics for rutile in various occurrences. The inclusion rutile (type 1) has limited variations of Nb/Ta ratios (14.9–17.2) and Nb (322.4–362.6 ppm), Ta (15.5–26.8 ppm), Zr (75–124 ppm), and Hf (2.8–3.7 ppm) contents (Figs. 9a, 9b, 9c, and 9f; Online Materials¹ Table OM3). The matrix rutile (type 2) has relatively higher Nb/Ta ratios (15.4–21.0) and Nb (324.3–483.8 ppm), Zr (96–248 ppm), and Hf (3.1–7.1 ppm) contents (Figs. 9a and 9f) than type 1 rutile. The megacrystal rutile in the veinlets (type 3) has slightly more scattered Nb/Ta ratios (13.9–22.5) and Ta contents (15.5–26.8 ppm; Fig. 9b), but relatively consistent Zr (72–105 ppm), Sc (1.1–2.4 ppm), Hf (3.3–4.5 ppm), and U (0.3–0.9 ppm, except for two analyses 6.1, 4.6 ppm) contents (Figs. 9d, 9e, and 9f; Online Materials¹ Table OM3).

We use the P -dependent Zr-in-rutile thermometry by Tomkins et al. (2007) to calculate temperature for rutile in various occurrences. Beforehand, P should be primarily constrained. The inclusion rutile (type 1) armored by garnet has a relatively consistent Zr content (Fig. 9c and may imply a system closed to Zr (Zhang et al. 2010). Therefore, we use a P of 25.0–30.0 kbar at the late prograde stage (Fig. 7f) for further calculation. The Zr content of 75.2–124.3 ppm results in T of 608–664 $^\circ C$ with the upper limit of the interquartile T range of 634–654 $^\circ C$ (Figs. 10a, 10c, and 10d). Matrix rutile (type 2) has been interpreted to coexist with the main rock-forming minerals (e.g., garnet and omphacite) at T_{max} or near T_{max} stages. Therefore, we calculate T for type 2 rutile at 25.0–20.0 kbar and the Zr content of 95.7–247.8 ppm resulting in T of 698–605 $^\circ C$ with the upper limit of the interquartile T

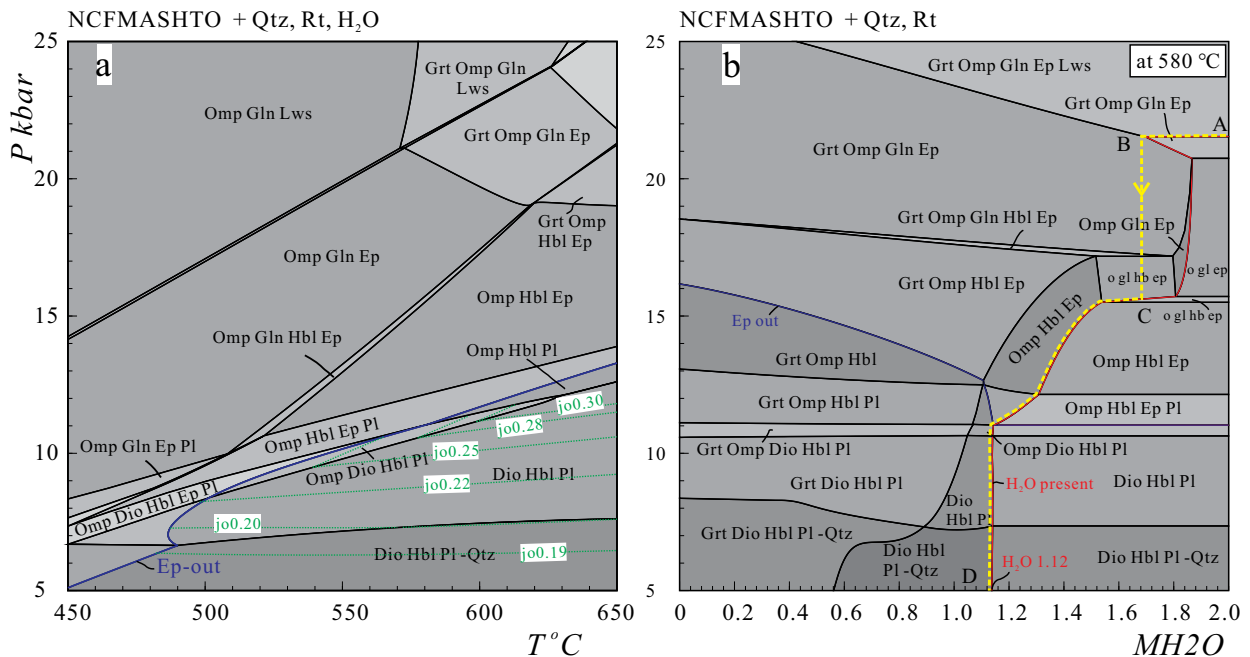
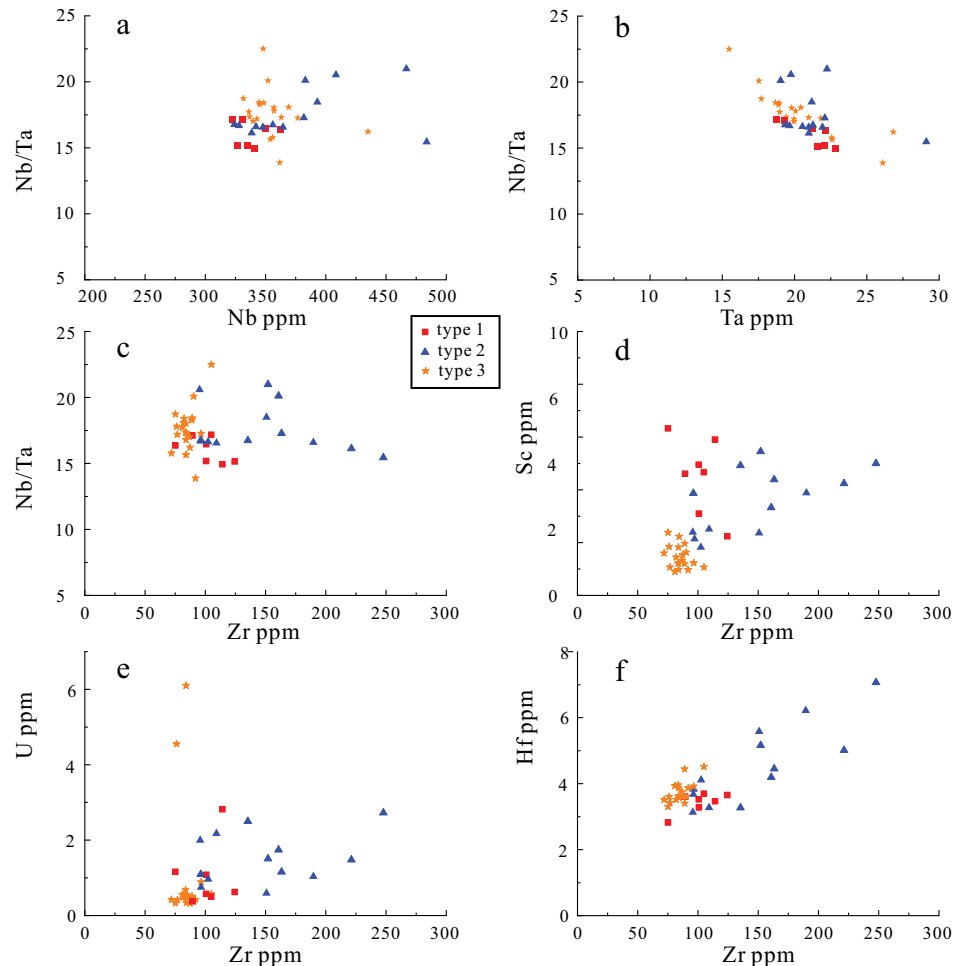


FIGURE 8. (a) P - T and (b) P - M_{H_2O} pseudosections for the eclogite Sdh-1. The whole-rock compositions are given in Table 1. “jo” represents calculated isopleths for $j(o)$ of omphacite. (Color online.)

FIGURE 9. (a–c) Nb/Ta vs. Nb, Ta, and Zr, and (d–f) Zr vs. Sc, U, and Hf characteristics for rutile with various occurrences. (Color online.)



range of 664–644 °C (Figs. 10a, 10c, and 10d). The megacrystal rutile (type 3) in the veinlet may be formed at a later stage at the transition of eclogite to amphibolite facies metamorphism (Zheng et al. 2011a). Therefore, we calculate T at 15.0–10.0 kbar and the Zr content of 71.9–105.0 ppm results in T of 592–548 °C with the upper limit of the interquartile T range of 581–561 °C (Figs. 10b, 10c, and 10d). The LA-ICP-MS analytical error for Zr in rutile is 4.7–16.6 ppm (within 2 sigma), corresponding to T uncertainties of 4–6 °C. However, following the recommendation of Tomkins et al. (2007), the uncertainty on T could be ~30 °C (within 2 sigma) using Zr-in-rutile thermometry. In this study, we adopt the upper limit of the interquartile T range for further discussion as recommended by Taylor-Jones and Powell (2015).

DISCUSSION

P-*T* evolution

Compositional isopleths including Grs, Prp, and X_{Mg} in garnet and j(o) of omphacite in eclogite are commonly used as *P*-*T* constraints in phase equilibrium modeling (Powell and Holland 2008; Wei et al. 2010; Groppo et al. 2015; Wang et al. 2021; Xia et al. 2018b, 2020). Although compositional re-equilibration could be expected at $T > 700$ °C (Caddick et al. 2010), modified garnet growth zonation has been identified in MT-UHP eclogite or even in granulite undergoing UHT metamorphic conditions

(e.g., O'Brien 1997; Schmid et al. 2000; Jiao et al. 2021). In this study, because of intense fluid activity during exhumation, the eclogites at Sidaohe in western Dabie have been retrograded during exhumation. However, in carefully selected samples, there are vestiges of prograde information preserved in large refractory porphyroblastic garnet. We interpret the obvious zoning of Ca in garnet to be original, thus, the fluctuations in Ca contents from core to rim may be due to *P* variations according to our phase equilibrium modeling. On the other hand, the weaker zoning of Mg, Fe, and X_{Mg} and lack of Mn zoning may be ascribed to partial diffusional re-equilibration during retrogression. The more obvious zoning of Ca than Mg, Fe, and Mn in large garnets may be due to the larger ionic radius of Ca and significantly more sluggish volume diffusion, according to numerical modeling (Chakraborty and Ganguly 1991; Schwandt et al. 1996; Vielzeuf et al. 2007).

When interpreting the results of phase equilibrium modeling, it is important to estimate the uncertainties which may comprise systematic and random uncertainties (Powell and Holland 2008; Xia et al. 2020). The systematic uncertainties on *P* and *T* propagated from each end-member enthalpy in the data set are calculated to be ±0.4 kbar and ±12 °C (2 sigma error) using Thermocalc, respectively. On the other hand, the random uncertainties propagated from the analytical uncertainties for EPMA (within ~2% relative) and the AX software for calculating mineral formulas

(~1–2% relative) could be ~0.6 kbar on P and ~10 °C on T (2 sigma error; Xia et al. 2020). Therefore, the absolute uncertainties on P are ± 1.0 kbar and on T are ± 20 °C (2 sigma error). However, we should take these values as minima if considering other systematic uncertainties propagated from a - x models and random uncertainties from the bulk rock composition.

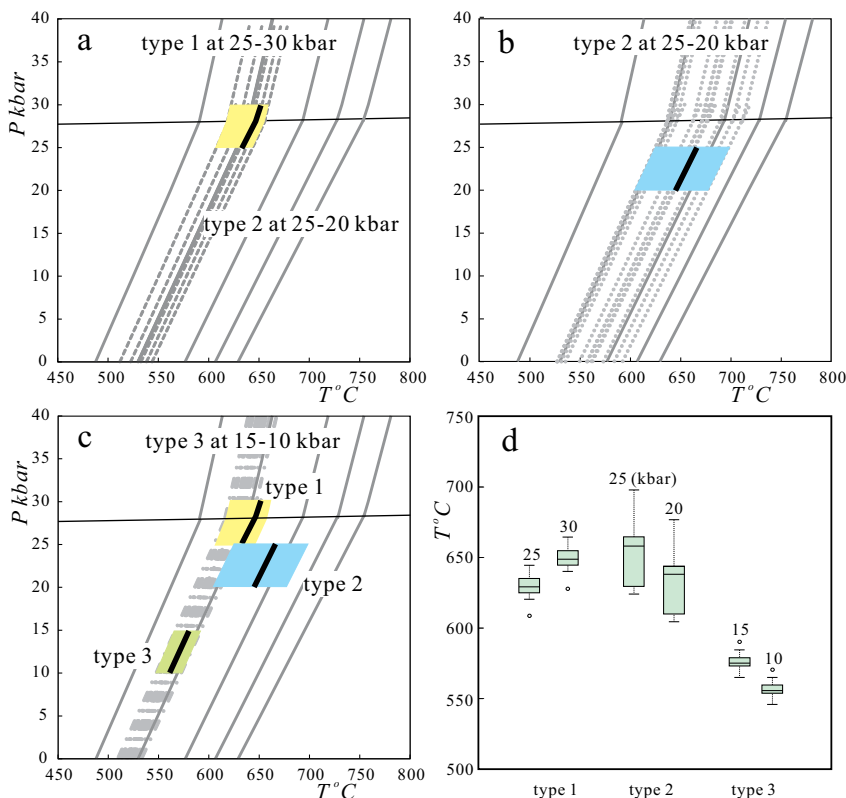
By combining the P - T results from phase equilibrium modeling, Amp-Pl thermobarometry and Zr-in-rutile thermometry, a complete P - T path is proposed for the eclogite at Sidaohe, western Dabie (Fig. 11), from the prograde stage to the peak stage, and then through several retrograde stages.

The prograde to P_{\max} stages. Based on inclusions of Omp + Amp + Ep + Qtz + Rt/Ilm in garnet and the composition of garnet and omphacite, we propose that the prograde P - T evolution (M0) passed through the modeled phase assemblage fields of Grt + Omp + Lws \pm Gln + Coe/Qtz + Rt + H₂O. Lawsonite and glaucophane have not been observed in the thin section, and most likely were replaced by epidote and calcium-rich amphibole (pargasite to tschermakite), respectively, during exhumation (Wei et al. 2010; Lou et al. 2013). Fractures around epidote and amphibole inclusions in garnet (Figs. 3a and 3b) may have acted as pathways for fluid infiltration to trigger retrogression. Based on garnet compositional isopleth thermobarometry, we propose an increase of P from 23.0 to 28.5 kbar, then a decrease to 24.0 kbar, before an increase to 30.5 kbar (± 1.0 kbar, 2 sigma error) concomitant with a small increase in T from 580 to 605 °C (± 20 °C, 2 sigma error; Figs. 7c, 7d, and 7e). However, since we are uncertain about the extent to which the Prp and X_{Mg} zoning profiles in garnet have been flattened, the T results based on Prp and X_{Mg} isopleths in

garnet should be treated with appropriate caution. Nevertheless, we infer two periods of compression separated by a period of decompression during the prograde evolution of the eclogite at Sidaohe, western Dabie (Figs. 7e and 7f). A compression path with a steep positive slope that reached P - T conditions for the P_{\max} stage of 29.0–30.5 kbar/590–605 °C are consistent with the results from an eclogite at Sibian about 20 km to the northwest in the same Xinxian UHP unit (Fig. 1b; Wei et al. 2010). This type of prograde evolution is similar to that modeled for oceanic crust in modern subduction zones due to coupling between the subducting slab and the overlying mantle wedge (e.g., model W1300; Syracuse et al. 2010), but at lower T and has been interpreted to represent fast subduction (Wei et al. 2010). The UHP metamorphism for the P_{\max} stage is consistent with the report of coesite pseudomorphs in eclogite at Sidaohe (Yan et al. 2005) and coesite in eclogite and the country rock gneisses in the Xinxian UHP unit (e.g., at Guojiahe and Chengmagang, Fig. 1; Zhang and Liou 1994; Liu et al. 2004, 2006). In the modeled phase assemblage field of Grt + Omp + Lws + Coe/Qtz + Rt + H₂O (Fig. 7d), a T of 595–650 °C (± 20 °C, 2 sigma error) at 25.0–30.0 kbar is constrained by isopleths of $j(o)$ of omphacite and is comparable to the T range of 634–654 °C (± 30 °C, 2 sigma error; here and subsequently, we use the upper limit of the interquartile range in T for the Zr-in-rutile thermometry results) recorded by rutile included in garnet (type 1), indicating a T increase after the P_{\max} stage (Fig. 10c).

The T_{\max} stage. Initial exhumation to the T_{\max} stage (M1) produced an inferred mineral assemblage of Grt + Omp + Coe/Qtz + Rt, which indicates the P - T evolution passed through the modeled phase assemblage fields of Grt + Omp + Coe/Qtz + Rt + H₂O after

FIGURE 10. The calculated T using the Zr-in-rutile thermometer by Tomkins et al. (2007) for rutile with various occurrences. (a) Calculated at 25.0–30.0 kbar for type 1 rutile. (b) Calculated at 25.0–20.0 kbar for type 2 rutile. (c) Calculated at 15.0–10.0 kbar for type 3 rutile and summary of the T calculated for rutile with various occurrences. (d) The interquartile T range for rutile with various occurrences. Box represents the interquartile T range. The thick black line in the rhombic field from a–c represents the upper limit of the interquartile T range. (Color online.)



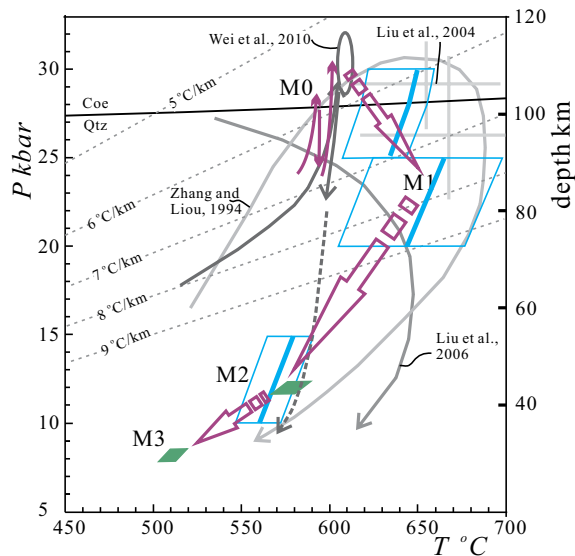


FIGURE 11. Summary of P - T paths from this and previous studies of eclogite from western Dabie. The purple arrows represent the P - T path from our study. The solid arrow was inferred from garnet compositional isopleth thermobarometry; the dashed arrow was inferred from a combination of phase equilibrium modeling, Zr-in-rutile thermometer (blue rhombus) and Hb-Pl thermobarometry (green diamond). (Color online.)

the P_{\max} stage (Figs. 7a and 7b). In these fields, the calculated modal contents of Grt and Omp are 47.0 and 36.7%, respectively, typical of the biomineral eclogite as observed in thin sections (Fig. 2c). For type 2 rutile in the matrix, using Zr-in-rutile thermometry we have calculated T of 664–644 °C (± 30 °C, 2 sigma error) at 25.0–20.0 kbar, interpreted to represent P - T conditions for the T_{\max} stage (Figs. 10c and 10d), similar to the results obtained using conventional thermobarometry by previous researchers (Zhang and Liou 1994; Liu et al. 2004). Along the P - T path from the P_{\max} to T_{\max} stages, Gln and Lws disappear via the reactions $\text{Lws} + \text{Omp} + \text{Gln} = \text{Grt} + \text{Qtz} + \text{H}_2\text{O}$ and $\text{Lws} + \text{Omp} \pm \text{Gln} = \text{Grt} + \text{Qtz} + \text{H}_2\text{O}$, respectively (Fig. 7f).

The retrograde stages. During subsequent exhumation, rock-forming omphacite in the matrix broke down to form Amp + Pl + Cpx symplectite (Sym1). Based on phase equilibrium modeling and conventional Amp-Pl thermometry, we estimate that Sym1 formed at 567–590 °C/12.0 kbar. This T range is similar to the T of 581–561 °C calculated at 15.0–10.0 kbar for type 3 rutile in the veinlets (Fig. 11). These P - T estimates are interpreted to represent a decrease of T during the retrograde stage M2 decompression. Late retrogression (M3) led to the formation of Sym3 at T of 504–520 °C, calculated at 8.0 kbar using Amp-Pl thermometry.

Summary. For eclogite at Sidaohe, western Dabie, we propose a P - T path with a prograde segment showing two cycles of P increase to the P_{\max} stage, then a T increase during initial exhumation to the T_{\max} stage, before a decrease in both P and T during subsequent retrograde stages. The clockwise, open convex P - T path is similar to those in the studies of Zhang and Liou (1994) and Liu et al. (2004, 2006) on eclogite from western Dabie, but differs from those in the studies of Wei et al. (2010) and Cheng and Cao (2015) who inferred isothermal decompression after the P_{\max} stage.

H₂O behavior along the P - T evolution

From the prograde to the P_{\max} stage. H₂O contents in the bulk rock are mainly controlled by the stability of hydrous minerals and the P - T fields related to various continuous and discontinuous reactions rock crossed during subduction (Schmidt and Poli 2014; Zheng and Chen 2016). In this study, P - T fields at 23.0–31.0 kbar (with Qz then Coe), 580–600 °C were constrained for a segment of the P - T evolution from the late prograde to P_{\max} stages (Fig. 7f). In these fields, previous experimental studies on metabasite compositions suggest that the hydrous minerals are mainly Lws, Ctd, Ph, and Ep/Zoi with Gln decomposed at $P > 23.0$ kbar (Schmidt and Poli 2014), while Wei and Zheng (2020) considered the stable minerals to be Lws, Ph, Amp, and Ta. In our study, due to the absence of significant K₂O and the low-MgO content in the bulk composition (Online Materials¹ Table OM3), Ph and Ta were not formed and H₂O in the bulk rock was retained only in Lws and Gln. Along the P - T path from A to B in Figure 7f, calculated modals of Gln decrease from 12.5 (A) to 0.3 (B) mode% whereas Lws slightly increase from 7.2 to 8.3 mode%. Accordingly, calculated H₂O content in the bulk rock slightly decreases from 0.92 to 0.88 wt%, implying the release of H₂O by the Gln-out reaction is compensated by an increase in modal Lws. Therefore, in subduction zones with low-thermal gradients (5–7 °C/Km), Lws in eclogites could be the most important H₂O reservoir. Indeed, it may take H₂O to 40.0 kbar at $T < 700$ °C, before destabilizing to form normally anhydrous garnet and omphacite (Schmidt and Poli 2014; Zheng and Chen 2016; Wei and Zheng 2020). In addition, numerous studies in Sulu-Dabie and elsewhere have shown that at UHP conditions, nominally anhydrous minerals (NAMs) such as Grt and Omp can incorporate a considerable amount of structural hydroxyl (OH⁻) and molecular water (H₂O) in point defects within the crystal lattice (Chen et al. 2007), allowing fluid to be carried into the deeper mantle (>200 km), and even to the mantle transition zone (Katayama and Nakashima 2003; Zheng 2009).

From the P_{\max} to T_{\max} stages. In Figure 7f, the P - T evolution from B to C sequentially crosses the Gln- and Lws-out curves and the modeled H₂O content for relevant assemblages rapidly decreases from 0.88 to 0 wt% (in the modeled assemblages there is no structural hydroxyl in the NAMs). Without considering hydroxyl/H₂O contained in NAMs, the eclogite would become biminerale and be effectively dry, consistent with our observations (Fig. 2c). The released H₂O may migrate out of the local rock system to promote crust-mantle interactions, the exhumation of deeply subducted continental crust, and the retrogression of HP/UHP rocks in continental subduction channels (Chen et al. 2007; Zheng and Chen 2016).

The retrograde stage. Strong fluid activity during the retrograde exhumation is evidenced by pervasive retrogression and the development of quartz veins/veinlets (Figs. 2c and 2d). During this process, H₂O may act as a kinetic facilitator for the destabilization of omphacite, as a component of the reaction to form amphibole in symplectite or as a carrier for components required to precipitate minerals in veinlets (Joanny et al. 1991; Martin 2019). For UHP eclogite, numerous studies have shown that H₂O may be released from the NAMs during retrograde exhumation (e.g., Chen et al. 2007; Zheng et al. 2011a). In Sulu-Dabie, the amount of structural hydroxyl could be 115–1300 ppm in omphacite and 92–1735 ppm

in garnet (Xia et al. 2005; Chen et al. 2007). The total H₂O concentration including fluid inclusions, hydrous mineral inclusions and structural hydroxyl could even be up to 1170–20745 ppm in Omphacite and 522–1584 ppm in garnet (Chen et al. 2007).

In this study, Sym2 at the reaction front with only rare or no Amp (Figs. 5c–5k) may require very little H₂O for its formation. By contrast, our modeling shows that Sym1, which has Amp several tens of micrometers in diameter (Figs. 5d–5g), requires a H₂O content of 0.4 wt% (or 4000 ppm) to hydrate the mineral assemblage (Fig. 8b). Considering Sym1 only developed at limited places around Sym2 (assumed <10 vol% in thin sections; Figs. 2c and 3g), we assume that a maximum H₂O content of 400 ppm in the bulk rock may be sufficient to the formation of Sym1. Such an amount of H₂O may be provided by H₂O released from the NAMs during decompression. Therefore, we interpret that the H₂O to trigger the formation of both Sym1 and Sym2 was internally sourced. A similar conclusion was reached by Anderson and Moecher (2007) and Martin (2019) in their studies of symplectite. In support of this interpretation in our study, rutile in the matrix (type 2) has comparable Ta, Sc, and U contents to rutile included in garnet (type 1; Figs. 9b, 9d, and 9e), implying the properties of fluid at this stage had an affinity with that forming type 1 rutile. The high-Zr and -Hf contents of the matrix rutile may be related to the breakdown of garnet.

The coarse-grained rutile (type 3) in veinlets has more scattered Nb/Ta ratios and Ta contents, but limited variation in Nb, Zr, and Hf contents, distinctly different from the inclusion rutile and the matrix rutile (Figs. 9a, 9b, and 9f), which may imply different properties of the metamorphic fluid compared with that at the prograde to peak stages (Zheng et al. 2011a). We interpret the rutile in veinlets to be formed from an external fluid source with constant Nb, Zr, and Hf contents but varied Ta content and Nb/Ta ratios. More abundant quartz veins developed at the transition zone of the eclogite block and the country rock gneisses may support this conclusion (Fig. 2a). The shear zone between the main interface of the eclogitic block and the country rock may act as a preferential path for fluid entering the rock during retrogression (cf. Martin 2019). Fluid may also promote the formation of Sym3 with coarse-grained Amp and Pl of comparable amount in the matrix, as has been evidenced by its more abundant development near the veinlets (Figs. 2b and 2d).

IMPLICATIONS

Polycyclic burial of eclogite in continental subduction channel

In this study, our modeling results show that eclogite within a single unit at Sidaohu records two cycles of *P* increase during the prograde metamorphic stage. The first cycle records a *P* increase from 23.0 to 28.5 kbar, followed by partial exhumation, and then a second cycle records a *P* increase from 24.0 to 30.5 kbar (Figs. 7e and 7f). Variations of the minimum to maximum *P* conditions for each cycle are up to 6.5 kbar, implying the two cycles of prograde *P* increase are a reliable result. The result is distinctly different from a single *P*-*T* loop commonly described for eclogite in Sulu-Dabie by previous studies (Zhang and Liou 1994; Liu et al. 2004; Cheng and Cao 2015; Wei et al. 2010; Xia et al. 2018a; Zheng et al. 2019).

In other places in the world, rocks showing *P* cycles during a single orogenic event have been reported and interpreted to repre-

sent burial-partial exhumation cycles (Brueckner 2006; Beltrando et al. 2007; Blanco-Quintero et al. 2011; Rubatto et al. 2011; Li et al. 2016). Overall, two scenarios have been proposed to interpret these cycles: (1) they are related to orogenic-scale shortening-extension switches mostly developed in the continental subduction environment (Brueckner 2006; Rubatto et al. 2011), and (2) they are developed within Franciscan-type subduction channels in oceanic subduction zones (Blanco-Quintero et al. 2011; Gerya et al. 2002; Li et al. 2016). In the first case, rocks showing short-term, multiple eclogite facies metamorphism from the Sesia zone in the Italian Western Alps were interpreted to be formed due to oblique subduction along the convergent plate margin. Episodic switches from transpressional to transtensional deformation led to alternating burial and partial exhumation for rocks in the subduction zone (Rubatto et al. 2011). In the second case, convective movement of rocks occurs within a thin and rapidly sheared layer of unconsolidated sediments (Lister et al. 2001) or serpentinites (Blanco-Quintero et al. 2011) mixed with fluid along the plate interface in the subduction channel (Cloos and Shreve 1988; Zheng et al. 2011b). The driving forces could be competing drag and buoyancy combined within a convecting fluid (Gerya et al. 2002; Blanco-Quintero et al. 2011; Zheng et al. 2012). For instance, eclogite from the Chinese western Tianshan records a polycyclic burial-partial exhumation evolution that was interpreted to be due to convective flow in the subduction channel (Li et al. 2016).

In this study, we interpret the multiple burials and partial exhumation cycles of eclogite at Sidaohu to be formed in a continental subduction channel. A crustal slice containing the eclogite may have been detached from the surface of the descending lower plate due to fracturing. After the crust had been subducted to a depth of ~100 km, a slice was detached and partially exhumed to ~82 km depth before being subducted again to a depth of ~107 km. This polycyclic movement may have proceeded due to convective flow in the channel. Metasedimentary rocks, well exposed in western Dabie, may have acted as a weak, low-viscosity material along the plate interface (Cloos and Shreve 1988; Lister et al. 2001; Gerya et al. 2002). In addition, dehydroxylation of NAMs and fluid ingress into eclogite, as discussed above, may facilitate convective movement of rock fragments in the continental subduction channel (Zheng et al. 2011b).

Our study indicates that information for polycyclic *P*-*T* evolution could be potentially preserved in garnet from low-*T* eclogite. Especially Ca may preserve prograde chemical variations considering its larger ionic size and lower diffusivity than the other divalent cations. By combining garnet zoning profiles and phase equilibrium modeling, we propose that more rocks showing polycyclic *P*-*T* evolution could be revealed in further studies.

Thermal relaxation during exhumation

The exhumation *P*-*T* path shows an increase in *T* from the P_{\max} to T_{\max} stages, followed by a decrease of both *P* and *T* (Fig. 11). The exhumation path depends on the balance between the rates of exhumation and temperature increase (Carswell and Zhang 1999). In the early stages of exhumation, unless the exhumation rate is exceedingly fast, deeply subducted rocks may continue to experience heating, resulting in the T_{\max} after the P_{\max} along the exhumation path (Carswell and Zhang 1999). Such a process has been anticipated by thermal modeling of subducted crustal

slabs (England and Thompson 1984). The increase in T after the P_{\max} is generally interpreted to be due to thermal relaxation by conductive heat transfer (Carswell and Zhang 1999; Winter 2013). For the deeply subducted continental crust, conductive heating driven by the relaxation of isotherms may operate on timescales of tens of millions of years (England and Thompson 1984). Large UHP terranes with ancient crustal protoliths may experience UHP metamorphism over long timescales with slow exhumation rates, while small UHP terranes commonly with juvenile crustal protoliths may experience UHP metamorphism over short timescales with rapid exhumation rates (Kylander-Clark et al. 2008; Zheng et al. 2019). As one of the largest UHP terranes on Earth, the Dabie-Sulu orogen has a metamorphic duration of 15 ± 2 Ma at subarc depths (Wu and Zheng 2013; Zheng et al. 2019). Therefore, in western Dabie, the relatively long duration of HP/UHP rocks at mantle depths may be sufficient for thermal relaxation during initial exhumation.

ACKNOWLEDGMENTS AND FUNDING

We thank associate editor David Dolejs and two anonymous reviewers for their helpful and constructive review comments that have substantially improved the manuscript and Michael Brown for his review of the original manuscript. This study was financially supported by the National Natural Science Foundation of China (41930215) and the Fundamental Research Funds for the Central Universities, China University of Geosciences (Wuhan).

REFERENCES CITED

- Anderson, E.D. and Moecher, D.P. (2007) Omphacite breakdown reactions and relation to eclogite exhumation rates. *Contributions to Mineralogy and Petrology*, 154, 253–277, <https://doi.org/10.1007/s00410-007-0192-x>.
- Beltrando, M., Hermann, J., Lister, G., and Compagnoni, R. (2007) On the evolution of orogens: Pressure cycles and deformation mode switches. *Earth and Planetary Science Letters*, 256, 372–388, <https://doi.org/10.1016/j.epsl.2007.01.022>.
- Blanco-Quintero, I.F., Garcia-Casco, A., and Gerya, T.V. (2011) Tectonic blocks in serpentinite mélange (eastern Cuba) reveal large-scale convective flow of the subduction channel. *Geology*, 39, 79–82, <https://doi.org/10.1130/G31494.1>.
- Bovary, T., Lanari, P., Rubatto, D., Smit, M., and Piccoli, F. (2021) Pressure-temperature-time evolution of subducted crust revealed by complex garnet zoning (Theodul Glacier Unit, Switzerland). *Journal of Metamorphic Geology*, <https://doi.org/10.1111/jmg.12623>.
- Bruckner, H.K. (2006) Dunk, dunkless and re-dunk tectonics: A model for metamorphism, lack of metamorphism, and repeated metamorphism of HP/UHP terranes. *International Geology Review*, 48, 978–995, <https://doi.org/10.2747/0020-6814.48.11.978>.
- Butler, J.P., Beaumont, C., and Jamieson, R.A. (2013) The Alps 1: A working geodynamic model for burial and exhumation of (ultra)high-pressure rocks in Alpine-type orogens. *Earth and Planetary Science Letters*, 377–378, 114–131, <https://doi.org/10.1016/j.epsl.2013.06.039>.
- Caddick, M.J., Konopásek, J., and Thompson, A.B. (2010) Preservation of garnet growth zoning and the duration of prograde metamorphism. *Journal of Petrology*, 51, 2327–2347, <https://doi.org/10.1093/petrology/egq059>.
- Carswell, D.A. and Zhang, R.Y. (1999) Petrographic characteristics and metamorphic evolution of ultrahigh-pressure eclogites in plate-collision Belts. *International Geology Review*, 41, 781–798, <https://doi.org/10.1080/00206819909465169>.
- Chakraborty, S. and Ganguly, J. (1991) Compositional zoning and cation diffusion in garnets. In J. Ganguly, Ed., *Diffusion, Atomic Ordering, and Mass Transport*, p. 120–175. Springer.
- Chen, R.X., Zheng, Y.F., Gong, B., Zhao, Z.F., Gao, T.S., Chen, B., and Wu, Y.B. (2007) Origin of retrograde fluid in ultrahigh-pressure metamorphic rocks: Constraints from mineral hydrogen isotope and water content changes in eclogite-gneiss transitions in the Sulu orogen. *Geochimica et Cosmochimica Acta*, 71, 2299–2325, <https://doi.org/10.1016/j.gca.2007.02.012>.
- Cheng, H. and Cao, D. (2015) Protracted garnet growth in high- P eclogite: Constraints from multiple geochronology and P - T pseudosection. *Journal of Metamorphic Geology*, 33, 613–632, <https://doi.org/10.1111/jmg.12136>.
- Cloos, M. and Shreve, R.L. (1988) Subduction-channel model of prism accretion, melange formation, sediment subduction, and subduction erosion at convergent plate margins: 2. Implications and discussion. *Pure and Applied Geophysics*, 128, 501–545, <https://doi.org/10.1007/BF00874549>.
- England, P.C. and Thompson, A.B. (1984) Pressure-temperature-time paths of regional metamorphism I. Heat transfer during the evolution of regions of thickened continental crust. *Journal of Petrology*, 25, 894–928, <https://doi.org/10.1093/petrology/25.4.894>.
- Gerya, T. and Stöckhert, B.S. (2006) Two-dimensional numerical modeling of tectonic and metamorphic histories at active continental margins. *International Journal of Earth Sciences*, 95, 250–274, <https://doi.org/10.1007/s00531-005-0035-9>.
- Gerya, T.V., Stöckhert, B., and Perchuk, A.L. (2002) Exhumation of high-pressure metamorphic rocks in a subduction channel: A numerical simulation. *Tectonics*, 21, 6–1–6–19.
- Godard, G. (2009) Two orogenic cycles recorded in eclogite-facies gneiss from the southern Armorican Massif (France). *European Journal of Mineralogy*, 21, 1173–1190, <https://doi.org/10.1127/0935-1221/2009/0021-1984>.
- Green, E.C.R., White, R.W., Diener, J.F.A., Powell, R., Holland, T.J.B., and Palin, R.M. (2016) Activity-composition relations for the calculation of partial melting equilibria in metabasic rocks. *Journal of Metamorphic Geology*, 34, 845–869, <https://doi.org/10.1111/jmg.12211>.
- Groppo, C., Rolfo, F., Liu, Y., Deng, L., and Wang, A. (2015) P-T evolution of elusive UHP eclogites from the Luotian dome (North Dabie Zone, China): How far can the thermodynamic modeling lead us? *Lithos*, 226, 183–200, <https://doi.org/10.1016/j.lithos.2014.11.013>.
- Hacker, B.R., Ratschbacher, L., Webb, L.E., McWilliams, M.O., Ireland, T., Calvert, A., Dong, S., Wenk, H.R., and Chateigner, D. (2000) Exhumation of ultrahigh-pressure continental crust in east central China: Late Triassic–Early Jurassic tectonic unroofing. *Journal of Geophysical Research*, 105 (B6), 13339–13364, <https://doi.org/10.1029/2000JB900039>.
- Harris, C.R., Hoisch, T.D., and Wells, M.L. (2007) Construction of a composite pressure-temperature path: Revealing the synorogenic burial and exhumation history of the Sevier hinterland, U.S.A.. *Journal of Metamorphic Geology*, 25, 915–934, <https://doi.org/10.1111/j.1525-1314.2007.00733.x>.
- Hawthorne, F.C., Oberti, R., Harlow, G.E., Maresch, W.V., Martin, R.F., Schumacher, J.C., and Welch, M.D. (2012) Nomenclature of the amphibole supergroup. *American Mineralogist*, 97, 2031–2048, <https://doi.org/10.2138/am.2012.4276>.
- Holland, T. and Blundy, J. (1994) Non-ideal interactions in calcic amphiboles and their bearing on amphibole-plagioclase thermometry. *Contributions to Mineralogy and Petrology*, 116, 433–447.
- Holland, T. and Powell, R. (2003) Activity-composition relations for phases in petrological calculations: An asymmetric multicomponent formulation. *Contributions to Mineralogy and Petrology*, 145, 492–501, <https://doi.org/10.1007/s00410-003-0464-z>.
- Holland, T.J.B. and Powell, R. (2011) An improved and extended internally consistent thermodynamic dataset for phases of petrological interest, involving a new equation of state for solids. *Journal of Metamorphic Geology*, 29, 333–383.
- Jiao, S., Evans, N.J., Guo, J., Fitzsimons, I.C.W., Zi, J., and McDonald, B.J. (2021) Establishing the P - T path of UHT granulites by geochemically distinguishing peritectic from retrograde garnet. *American Mineralogist*, 106, 1640–1653, <https://doi.org/10.2138/am-2021-7681>.
- Joanny, V., Van Roermund, H., and Lardeaux, J.M. (1991) The clinopyroxene/plagioclase symplectite in retrograde eclogites: A potential geothermobarometer. *Geologische Rundschau*, 80, 303–320, <https://doi.org/10.1007/BF01829368>.
- Katayama, I. and Nakashima, S. (2003) Hydroxyl in clinopyroxene from the deep subducted crust: Evidence for H_2O transport into the mantle. *American Mineralogist*, 88, 229–234, <https://doi.org/10.2138/am-2003-0126>.
- Kylander-Clark, A.R.C., Hacker, B.R., and Mattinson, J.M. (2008) Slow exhumation of UHP terranes: Titanite and rutile ages of the Western Gneiss Region, Norway. *Earth and Planetary Science Letters*, 272, 531–540, <https://doi.org/10.1016/j.epsl.2008.05.019>.
- Lanari, P., Riel, N., Guillot, S., Vidal, O., Schwartz, S., Pecher, A., and Hattori, K.H. (2013) Deciphering high-pressure metamorphism in collisional context using microprobe mapping methods: Application to the Stak eclogitic massif (northwest Himalaya). *Geology*, 41, 111–114, <https://doi.org/10.1130/G33523.1>.
- Li, J.L., Klemd, R., Gao, J., and John, T. (2016) Poly-cyclic metamorphic evolution of eclogite: Evidence for multistage burial-exhumation cycling in a subduction channel. *Journal of Petrology*, 57, 119–146, <https://doi.org/10.1093/petrology/egw002>.
- Li, Z., Li, Y., Wijbrans, J.R., Yang, Q., Qiu, H., and Brouwer, F.M. (2018) Metamorphic P - T path differences between the two UHP terranes of Sulu orogen, eastern China: Petrologic comparison between eclogites from Donghai and Rongcheng. *Journal of Earth Science*, 29, 1151–1166, <https://doi.org/10.1007/s12583-018-0845-x>.
- Liou, J.G., Tsujimori, T., Zhang, R.Y., Katayama, I., and Maruyama, S. (2004) Global UHP metamorphism and continental subduction/collision: the Himalayan model. *International Geology Review*, 46(1), 1–27.
- Lister, G.S., Forster, M.A., and Rawling, T.J. (2001) Episodicity during orogenesis. In J.A. Miller, R.E. Holdsworth, I.S. Buick, and M. Hand, Eds., *Continental Reactivation and Reworking*, 184, p. 89–113. Geological Society of London.
- Liu, X., Jahn, B., Liu, D., Dong, S., and Li, S. (2004) SHRIMP U-Pb zircon dating of a metagabbro and eclogites from western Dabieshan (Hong'an Block), China, and its tectonic implications. *Tectonophysics*, 394, 171–192, <https://doi.org/10.1016/j.tecto.2004.08.004>.
- Liu, J., Ye, K., and Sun, M. (2006) Exhumation P - T path of UHP eclogites in the Hong'an area, western Dabie Mountains, China. *Lithos*, 89, 154–173, <https://doi.org/10.1016/j.lithos.2005.12.002>.
- Liu, Y.S., Hu, Z.C., Gao, S., Günther, D., Xu, J., Gao, C.G., and Chen, H.H. (2008) In situ analysis of major and trace elements of anhydrous minerals by LA-ICP-MS without applying an internal standard. *Chemical Geology*, 257, 34–43, <https://doi.org/>

- 10.1016/j.chemgeo.2008.08.004.
- Liu, X.C., Wu, Y.B., Gao, S., Wang, J., Peng, M., Gong, H.J., Liu, Y.S., and Yuan, H.L. (2011) Zircon U-Pb and Hf evidence for coupled subduction of oceanic and continental crust during the Carboniferous in the Huwan shear zone, western Dabie orogen, central China. *Journal of Metamorphic Geology*, 29, 233–249, <https://doi.org/10.1111/j.1525-1314.2010.00914.x>.
- Lou, Y., Wei, C., Liu, X., Zhang, C., Tian, Z., and Wang, W. (2013) Metamorphic evolution of garnet amphibolite in the western Dabieshan eclogite belt, Central China: Evidence from petrography and phase equilibria modeling. *Journal of Asian Earth Sciences*, 63, 130–138, <https://doi.org/10.1016/j.jseas.2012.11.031>.
- Martin, C. (2019) *P-T* conditions of symplectite formation in the eclogites from the Western Gneiss Region (Norway). Special Publication, Geological Society of London, 478, 197–216, <https://doi.org/10.1144/SP478.18>.
- Morimoto, N., Fabries, J., Ferguson, A.K., Ginzburg, I.V., Ross, M., Seifert, F.A., Zussman, J., Aoki, K., and Gottardi, G. (1988) Nomenclature of pyroxenes. *American Mineralogist*, 73(9-10), 1123–1133.
- O'Brien, P.J. (1997) Garnet zoning and reaction textures in overprinted eclogites, Bohemian Massif, European variscides: A record of their thermal history during exhumation. *Lithos*, 41, 119–133, [https://doi.org/10.1016/S0024-4937\(97\)82008-7](https://doi.org/10.1016/S0024-4937(97)82008-7).
- Powell, R. and Holland, T.J.B. (2008) On thermobarometry. *Journal of Metamorphic Geology*, 26(2), 155–179.
- Ratschbacher, L., Franz, L., Jonckheere, R., Porschke, A., Hacker, B., Dong, S., and Zhang, Y. (2006) The Sino Korean-Yangtze suture, the Huwan detachment, and the Paleozoic-Tertiary exhumation of (ultra)high-pressure rocks along the Tongbai-Xinxian-Dabie Mountains. *Geological Society of America Bulletin*, 403, 45–75.
- Rubatto, D., Regis, D., Hermann, J., Boston, K., Engi, M., Beltrando, M., and McAlpine, S.R.B. (2011) Yo-yo subduction recorded by accessory minerals in the Italian Western Alps. *Nature Geoscience*, 4, 338–342, <https://doi.org/10.1038/ngeo1124>.
- Schmid, R., Franz, L., Oberhänsli, R., and Dong, S. (2000) High-Si phengite, mineral chemistry and *P-T* evolution of ultra-high-pressure eclogites and calc-silicates from the Dabie Shan, eastern China. *Geological Journal*, 35, 185–207, <https://doi.org/10.1002/gj.863>.
- Schmidt, M. (1992) Amphibole composition in tonalite as a function of pressure: An experimental calibration of the Al-in-hornblende barometer. *Contributions to Mineralogy and Petrology*, 110, 304–310, <https://doi.org/10.1007/BF00310745>.
- Schmidt, M.W. and Poli, S. (2014) Devolatilization during subduction. In H.D. Holland and K.K. Turekian, Eds., *Treatise on Geochemistry*, 2nd ed., 4, p. 669–701. Elsevier.
- Schwandt, C.S., Cygan, R.T., and Westrich, H.R. (1996) Ca self-diffusion in grossular garnet. *American Mineralogist*, 81, 448–451, <https://doi.org/10.2138/am-1996-3-418>.
- Shreve, R.L. and Cloos, M. (1986) Dynamics of sediment subduction, mélange formation, and prism accretion. *Journal of Geophysical Research*, 91 (B10), 10229–10245, <https://doi.org/10.1029/JB091iB10p10229>.
- Suo, S., Zhong, Z., Zhou, H., You, Z., and Zhang, L. (2012) Two fresh types of eclogites in the Dabie-Sulu UHP metamorphic belt, China: Implications for the deep subduction and earliest stages of exhumation of the continental crust. *Journal of Earth Science*, 23, 775–785, <https://doi.org/10.1007/s12583-012-0295-9>.
- Syracuse, E.M., van Keken, P.E., and Abers, G.A. (2010) The global range of subduction zone thermal models. *Physics of the Earth and Planetary Interiors*, 183, 73–90, <https://doi.org/10.1016/j.pepi.2010.02.004>.
- Taylor-Jones, K. and Powell, R. (2015) Interpreting zirconium-in-rutile thermometric results. *Journal of Metamorphic Geology*, 33, 115–122, <https://doi.org/10.1111/jmg.12109>.
- Tomkins, H.S., Powell, R., and Ellis, D.J. (2007) The pressure dependence of the zirconium-in-rutile thermometer. *Journal of Metamorphic Geology*, 25, 703–713, <https://doi.org/10.1111/j.1525-1314.2007.00724.x>.
- Vielzeuf, D., Baronnet, A., Perchuk, A.L., Laporte, D., and Baker, M.B. (2007) Calcium diffusivity in aluminosilicate garnets: An experimental and ATEM study. *Contributions to Mineralogy and Petrology*, 154, 153–170, <https://doi.org/10.1007/s00410-007-0184-x>.
- Wang, J.M., Lanari, P., Wu, F.Y., Zhang, J.J., Khanal, G.P., and Yang, L. (2021) First evidence of eclogites overprinted by ultrahigh temperature metamorphism in Everest East, Himalaya: Implications for collisional tectonics on early Earth. *Earth and Planetary Science Letters*, 558, 116760, <https://doi.org/10.1016/j.epsl.2021.116760>.
- Waters, D. (2003) *P-T* path from Cpx-Hbl-Pl symplectites, updated January 9, 2007. <http://www.earth.ox.ac.uk/~davewa/research/eclogites/symplectites.html> (Accessed July 2012).
- Wei, C. and Zheng, Y. (2020) Metamorphism, fluid behavior and magmatism in oceanic subduction zones. *Science China. Earth Sciences*, 63, 52–77, <https://doi.org/10.1007/s11430-019-9482-y>.
- Wei, C.J., Li, Y.J., Yu, Y., and Zhang, J.S. (2010) Phase equilibria and metamorphic evolution of glaucophane-bearing UHP eclogites from the Western Dabieshan Terrane, Central China. *Journal of Metamorphic Geology*, 28, 647–666, <https://doi.org/10.1111/j.1525-1314.2010.00884.x>.
- White, R.W., Powell, R., Holland, T.J.B., Johnson, T.E., and Green, E.C.R. (2014) New mineral activity-composition relations for thermodynamic calculations in metapelite systems. *Journal of Metamorphic Geology*, 32, 261–286, <https://doi.org/10.1111/jmg.12071>.
- Whitney, D.L. and Evans, B.W. (2010) Abbreviations for names of rock-forming minerals. *American Mineralogist*, 95, 185–187, <https://doi.org/10.2138/am.2010.3371>.
- Winter, J.D. (2013) *Principles of Igneous and Metamorphic Petrology*, 720 p. Pearson Prentice Hall.
- Wu, Y. and Zheng, Y. (2013) Tectonic evolution of a composite collision orogen: An overview on the Qinling-Tongbai-Hong'an-Dabie-Sulu orogenic belt in central China. *Gondwana Research*, 23, 1402–1428, <https://doi.org/10.1016/j.gr.2012.09.007>.
- Wu, Y., Hancher, J.M., Gao, S., Sylvester, P.J., Tubrett, M., Qiu, H., Wijbrans, J.R., Brouwer, F.M., Yang, S., Yang, Q., and others. (2009) Age and nature of eclogites in the Huwan shear zone, and the multi-stage evolution of the Qinling-Dabie-Sulu orogen, central China. *Earth and Planetary Science Letters*, 277, 345–354, <https://doi.org/10.1016/j.epsl.2008.10.031>.
- Xia, Q.K., Sheng, Y.M., Yang, X.Z., and Yu, H.M. (2005) Heterogeneity of water in garnets from UHP eclogites, eastern Dabieshan, China. *Chemical Geology*, 224, 237–246, <https://doi.org/10.1016/j.chemgeo.2005.08.003>.
- Xia, B., Brown, M., Wang, L., Wang, S., and Piccoli, P. (2018a) Phase equilibrium modeling of MT-UHP eclogite: A case study of coesite eclogite at Yangkou Bay, Sulu Belt, Eastern China. *Journal of Petrology*, 59, 1253–1280, <https://doi.org/10.1093/petrology/egy060>.
- Xia, B., Yang, Q., Chen, N., and Zhou, Z. (2018b) Phase equilibrium modeling of retrograded eclogite at the Kekesu Valley, Eastern Segment of SW Tianshan Orogen and Tectonic Implications. *Journal of Earth Science*, 29, 1060–1073, <https://doi.org/10.1007/s12583-018-0844-y>.
- Xia, B., Brown, M., and Zhang, L. (2020) *P-T* evolution and tectonic significance of lawsonite-bearing schists from the eastern segment of the southwestern Tianshan, China. *Journal of Metamorphic Geology*, 38, 935–962, <https://doi.org/10.1111/jmg.12555>.
- Yan, Q., Zhong, Z., and Zhou, H. (2005) Petrology of Sidaohe area in the UHP metamorphic terrane, the Dabie Mountains. *Acta Petrologica et Mineralogica*, 24, 186–196 (in Chinese with English abstract).
- Zhang, R. and Liou, J.G. (1994) Coesite-bearing eclogite in Henan Province, central China: Detailed petrography, glaucophane stability and *P-T* path. *European Journal of Mineralogy*, 6, 217–234, <https://doi.org/10.1127/ejm/6/2/0217>.
- Zhang, R.Y., Liou, J.G., and Ernst, W.G. (2009) The Dabie-Sulu continental collision zone: A comprehensive review. *Gondwana Research*, 16(1), 1–26.
- Zhang, G., Ellis, D.J., Christy, A.G., Zhang, L., and Song, S. (2010) Zr-in-rutile thermometry in HP/UHP eclogites from Western China. *Contributions to Mineralogy and Petrology*, 160, 427–439, <https://doi.org/10.1007/s00410-009-0486-2>.
- Zheng, Y.F. (2009) Fluid regime in continental subduction zones: Petrological insights from ultrahigh-pressure metamorphic rocks. *Journal of the Geological Society*, 166, 763–782, <https://doi.org/10.1144/0016-76492008-016R>.
- Zheng, Y. and Chen, Y. (2016) Continental versus oceanic subduction zones. *National Science Review*, 3, 495–519, <https://doi.org/10.1093/nsr/nww049>.
- Zheng, Y.F., Gao, X.Y., Chen, R.X., and Gao, T.S. (2011a) Zr-in-rutile thermometry of eclogite in the Dabie orogen: Constraints on rutile growth during continental subduction-zone metamorphism. *Journal of Asian Earth Sciences*, 40, 427–451, <https://doi.org/10.1016/j.jseas.2010.09.008>.
- Zheng, Y.F., Xia, Q.X., Chen, R.X., and Gao, X.Y. (2011b) Partial melting, fluid supercriticality and element mobility in ultrahigh-pressure metamorphic rocks during continental collision. *Earth-Science Reviews*, 107, 342–374, <https://doi.org/10.1016/j.earscirev.2011.04.004>.
- Zheng, Y.F., Zhang, L.F., McClelland, W.C., and Cuthbert, S. (2012) Processes in continental collision zones: Preface. *Lithos*, 136–139, 1–9, <https://doi.org/10.1016/j.lithos.2011.11.020>.
- Zheng, Y., Zhao, Z., and Chen, R. (2019) Ultrahigh-pressure metamorphic rocks in the Dabie-Sulu orogenic belt: Compositional inheritance and metamorphic modification. Special Publication, Geological Society of London, 474, 89–132, <https://doi.org/10.1144/SP474.9>.

MANUSCRIPT RECEIVED JANUARY 9, 2022

MANUSCRIPT ACCEPTED AUGUST 17, 2022

ACCEPTED MANUSCRIPT ONLINE SEPTEMBER 2, 2022

MANUSCRIPT HANDLED BY DAVID DOLEIS

Endnote:

¹Deposit item AM-23-78446, Online Materials. Deposit items are free to all readers and found on the MSA website, via the specific issue's Table of Contents (go to http://www.minsocam.org/MSA/AmMin/TOC/2023/Jul2023_data/Jul2023_data.html).